Published online 16 May 2016

Nucleic Acids Research, 2016, Vol. 44, No. 13 **6213–6231**
doi: 10.1093/nar/gkw349

G-rich telomeric and ribosomal DNA sequences from the fission yeast genome form stable G-quadruplex DNA structures *in vitro* and are unwound by the Pfh1 DNA helicase

Marcus Wallgren, Jani B. Mohammad†, Kok-Phen Yan†, Parham Pourbozorgi-Langroudi, Mahsa Ebrahimi and Nasim Sabouri*

Department of Medical Biochemistry and Biophysics, Umeå University, SE-901 87, Umeå, Sweden

Received February 2, 2016; Revised April 19, 2016; Accepted April 19, 2016

ABSTRACT

Certain guanine-rich sequences have an inherent propensity to form G-quadruplex (G4) structures. G4 structures are e.g. involved in telomere protection and gene regulation. However, they also constitute obstacles during replication if they remain unresolved. To overcome these threats to genome integrity, organisms harbor specialized G4 unwinding helicases. In *Schizosaccharomyces pombe*, one such candidate helicase is Pfh1, an evolutionarily conserved Pif1 homolog. Here, we addressed whether putative G4 sequences in *S. pombe* can adopt G4 structures and, if so, whether Pfh1 can resolve them. We tested two G4 sequences, derived from *S. pombe* ribosomal and telomeric DNA regions, and demonstrated that they form inter- and intramolecular G4 structures, respectively. Also, Pfh1 was enriched *in vivo* at the ribosomal G4 DNA and telomeric sites. The nuclear isoform of Pfh1 (nPfh1) unwound both types of structure, and although the G4-stabilizing compound Phen-DC$_3$ significantly enhanced their stability, nPfh1 still resolved them efficiently. However, stable G4 structures significantly inhibited adenosine triphosphate hydrolysis by nPfh1. Because ribosomal and telomeric DNA contain putative G4 regions conserved from yeasts to humans, our studies support the important role of G4 structure formation in these regions and provide further evidence for a conserved role for Pif1 helicases in resolving G4 structures.

INTRODUCTION

DNA molecules can adopt a diverse array of different structures. G-quadruplex (G4) DNA structures are a type of stacked secondary structure stabilized by monovalent cations and held together by non-canonical Hoogsteen base pairing between four guanine bases (1). G-rich sequences with the potential to form G4 structures (termed G4 motifs), give rise to a great diversity of G4 structures because the structures can be folded inter- and intramolecularly, and can form parallel, antiparallel and hybrid topologies (1). Also, the number of stacked G-quartets and the size and the sequence of the resulting loops can vary (1). G4 motifs are found in various genomes, and they are not randomly distributed but are instead enriched at specific genomic features in evolutionarily divergent organisms, suggesting that predicted G4 structures have important cellular functions (2–6). For example, in *Schizosaccharomyces pombe*, *Saccharomyces cerevisiae* and human cells, G4 motifs are enriched in several common genomic features such as the telomeres, ribosomal DNA (rDNA) and promoter regions (2–3,6–9). A recent study using high-throughput sequencing estimated that about 700 000 G4 motifs exist in the human genome (10). In human cell cultures, the formation of G4 structures can be visualized with G4-specific antibodies in both telomeres and at internal chromosomal regions (11,12). However, the total number of G4 structures as well as the moment of their formation *in vivo* are still unresolved questions.

S. pombe is a commonly studied model organism because of its many similar chromosomal features to human cells (13). Similar to human chromosomes, *S. pombe* telomeres and rDNA regions are enriched with G4 motifs (7). The enrichment of G4 motifs and formation of G4 structures at telomeres are proposed to be important for protecting telomeres and for regulating telomerase activity (14,15). The evolutionary conservation of G4 motifs in rDNA suggests that these sequences play a functional role in the

*To whom correspondence should be addressed. Tel: +46 90 786 50 00; Fax: +46 90 786 97 95; Email: nasim.sabouri@umu.se
† These authors contributed equally to the paper.

rDNA and/or rRNA (2,37,9). The density of G4 motifs at *S. pombe* telomeres and rDNA is 20-fold and 12-fold higher, respectively, than the rest of the nuclear genome (7). The major G4-enriched region in *S. pombe*, the telomeres, has ∼4.5 G4 motifs per kb (7). In each *S. pombe* rDNA repeat, all five G4 motifs are located on the non-transcribed strand, and the roughly 300 rDNA repeats make up about 1500 G4 motifs in the rDNA region (7).

Several human helicases, such as WRN, FANCJ, BLM and PIF1 (hPIF1), are G4-binding helicases that are linked to genetic diseases (16–18). For example, the WRN helicase is associated with Werner syndrome, FANCJ with Fanconi anemia and hPIF1 with familial breast cancer (16,18). hPIF1 belongs to the evolutionarily conserved Pif1 family, which comprises multifunctional helicases with a unique 21 amino acid signature motif (19). In contrast to *S. cerevisiae*, which encodes two well-studied Pif1 family helicases (ScPif1 and ScRrm3), Pfh1 is the sole *S. pombe* Pif1 member (19). An unresolved question has been whether organisms encoding one Pif1 helicase, such as *S. pombe* and humans, encode a helicase that has a more ScPif1-like or ScRrm3-like function. Both ScPif1 and ScRrm3 play important but divergent roles in genome stability (19), and the only known overlapping function of these two helicases is to resolve putative G4 structures *in vivo* (20), where ScRrm3 can substitute for ScPif1 as detected by elevated gross chromosomal rearrangements induced by G4 motifs in *pif1-m2 rrm3Δ* cells compared to *pif1-m2* cells (20).

The known functions of Pfh1 are in some ways close to ScRrm3 and in other ways close to ScPif1. For example, Pfh1 and ScRrm3 both promote replication at hard-to replicate regions, such as at telomeres, highly transcribed RNA polymerase III genes and replication fork barriers at the rDNA and mating-type loci (21–24), whereas Pfh1 and ScPif1 promote fork progression and suppress genomic instability at G4 motifs (7,20,25–28). However, other activities, such as promoting fork progression at highly transcribed RNA polymerase II genes, is only performed by Pfh1 (21).

Pfh1 has mitochondrial and nuclear isoforms, and both isoforms are essential for viability (29). About 20% of the predicted G4 structures are bound by Pfh1, and fork progression is slowed down or paused at these motifs in Pfh1-depleted cells leading to an increase in DNA damage due to fork breakage (7), indicating that Pfh1 promotes fork progression by unwinding these structures. These observations led us to ask if the conserved putative *S. pombe* G4 motifs fold into G4 structures and whether Pfh1 possesses the conserved ability to unwind stable G4 structures *in vitro*. Recombinantly expressed ScPif1, hPIF1 and several bacterial Pif1 helicases can unwind G4 structures *in vitro* (17,20,30), a property that might be intrinsic to all Pif1 family helicases. However, due to solubility and protein stability issues the G4 unwinding activities of recombinant full-length ScRrm3 (22) and Pfh1 (31–33) have not yet been tested.

Here, we present the first evidence that G4 motifs from *S. pombe* rDNA and telomeres form predominantly inter- and intramolecular G4 structures, respectively, and we also successfully purified the nuclear isoform of Pfh1 (nPfh1) and found that it was able to unwind these structures. The recombinant protein even efficiently resolved G4 structures treated with the G4-stabilizing compound Phen-DC_3. In addition, our *in vivo* data demonstrated that Pfh1 was enriched at telomeres and rDNA G4 motifs. Our work provide further evidence that unwinding G4 structures to preserve genome stability is a conserved task for the Pif1 family helicases.

MATERIALS AND METHODS

Preparation of the G4 DNA

The candidate G4 structures tested here were derived from the G4 motif-enriched rDNA and telomeric regions in *S. pombe* reported in Sabouri *et al.* (7), and were predicted with the $(G_{\geq 3}\ N_{1\text{-}25})_3\ G_{\geq 3}$ algorithm, i.e. four runs with a minimum of three guanines separated by loop regions up to 25 nt in length (2,7). To produce G4 DNA structures, 50 μM of a G4 oligonucleotide (MWG-Biotech AG; see Supplementary Table S1) was heated at 95°C for 5 min in a buffer containing 10 mM Tris/HCl (pH 7.5) with 100 mM NaCl or KCl or with 1 M NaCl or KCl followed by slow cooling to room temperature.

Circular dichroism (CD) spectroscopy

The secondary structures of the G4 DNA were analyzed using a JASCO J-710 Spectropolarimeter (JASCO) equipped with a Peltier element for temperature control. To perform the CD measurements, the folded oligonucleotides were diluted to 5 μM in 10 mM Tris/HCl (pH 7.5), 1.25% (v/v) DMSO and 100 mM NaCl/KCl in the absence or presence of 25 μM of the bisquinolinium G4 ligand Phen-DC_3. The samples were put into a 1 mm path length quartz cuvette (Hellma) and spectra were collected from 225 to 325 nm at 25, 45, 65 and 85°C using the following parameters: 0.5 nm data pitch, continuous, 50 nm/min scanning speed, 1 s response, 2 nm bandwidth, 4 spectra accumulations and 100 millidegrees (mdegs) standard sensitivity. The background from the buffer was corrected using a sample containing no DNA. For the determination of the molecularity of the G4 structures, see Supplementary Materials and Methods.

Thioflavin T (ThT) assay

A 20 μl mixture containing 1 μM oligonucleotide, 0.5 μM ThT, 50 mM Tris/HCl (pH 7.5) and 50 mM KCl or NaCl was added into a black Corning flat-bottom 384-well plate (Sigma-Aldrich) for fluorescence measurement using an Infinite M200 plate reader (TECAN). The data were acquired using the following parameters: 435 nm excitation wavelength, 480 nm emission wavelength, 0 μs lag time, 20 μs integration time, 25 flashes and optimal gain. After correcting the measured fluorescence values with a blank (buffer only), the FI/FI0 parameter was calculated for each sample by dividing the fluorescence value of ThT in the presence of DNA (FI) by the fluorescence value of ThT in the absence of DNA (FI0) (34).

Chromatin immunoprecipitation (ChIP) analysis

The ChIP experiments were performed in either *cdc25-22* (yNS76), *cdc25-22 ura4-D18 his3-D1 leu1-*

32::PJK148-pfh1-13MYC-kanmx6 cdc20::cdc20-3HA-kanmx6 (yNS102) or *cdc25-22 leu1-32::PJK148-pfh1-13MYC-kanmx6 cdc20::cdc20-3HA-kanmx6* (yNS103) cells and were performed in both synchronous, asynchronous and G2-arrested cells. For the asynchronous samples, the cells were grown at the permissive temperature of 25°C until reaching 8×10^6 cells/ml at which time they were crosslinked in 1% formaldehyde for 5 min. To prepare G2-arrested cells, the cell cultures were quickly shifted from 25 to 36°C when reaching 6×10^6 cells/ml. After a 5-h incubation at 36°C, the cultures were rapidly cooled down to 25°C and crosslinked in 1% formaldehyde for 5 min. The ChIP experiments were performed as described previously (21). Briefly, chromatin was sheared with a Covaris E220 system to an average of ∼300 bp, and Pfh1-13Myc or the untagged strain was immunoprecipitated with an anti-Myc antibody (Clontech, catalog number 631206). Both input and immunoprecipitated DNA were purified and quantified by quantitative polymerase chain reaction (qPCR) (Lightcycler® 96, Roche Life Science) using primer pairs for the *gal1*$^+$ gene, the rDNA G4 (located on chromosome III with the coordinates 3655-3679, 14 525-14 549 and 2 449 595-2 449 619) and the subtelomeres (Supplementary Table S2). The coordinates are from *S. pombe* genome assembly ASM294v2. To perform ChIP on synchronous cell cultures, 6×10^6 cells/ml were arrested in G2 phase as described above and released by shifting the cells to 25°C. Samples were crosslinked at 0, 20, 40, 60, 72, 84, 96, 108, 120, 140 and 160 min after the release. At these time points, samples for fluorescence-activated cell sorting (FACS) analysis were also collected to monitor the cell cycle progression. ChIP-qPCR was performed as described for asynchronous and G2 phase cells. The experiment was repeated two times.

Expression and purification of nPfh1

nPfh1 was amplified from *S. pombe* cDNA by PCR using the oligonucleotides 5′-GCT ACC ATG GGG TTT CAA AGA GCT CAG CAG AAA AG-3′ and 5′-GCT TGG TAC CTT ACT TAT TTT TGA CTC CCC TCA TTT G-3′. The PCR product was subsequently cloned into a series of pET vectors based on a modified pET-22 vector to express nPfh1 fused to various His_6-tagged carrier proteins at the N-terminus under the control of the T7 promoter. We tested the expression of the different constructs by varying the induction time and temperature as well as the isopropyl-β-D-1-thiogalactopyranoside (IPTG) concentration, and the construct expressing nPfh1 fused to His_6-thioredoxin (His_6-Trx) resulted in the greatest yield of soluble protein. To further facilitate subsequent purification, a sequence encoding a C-terminal FLAG-tag was added by PCR to create a double tagged protein, His_6-Trx-nPfh1-FLAG. From here on, the His_6-Trx-nPfh1-FLAG construct will be referred to simply as nPfh1. As a control to ensure that no helicase activity was present from contaminating proteins that might have remained after purification, the adenosine triphosphatase (ATPase)-inactive Pfh1 variant His_6-Trx-nPfh1-K338A-FLAG (nPfh1-K338A; lysine to alanine substitution at position 338 in the protein encoded by its full-length open reading frame (ORF)) was created by PCR and cloned into the same vector as the wild-type protein.

After transforming Rosetta™ 2 (DE3) cells with the plasmid, the cells were grown in LB medium containing 50 μg/ml kanamycin and 34 μg/ml chloramphenicol at 37°C until the OD_{600} was ∼0.6. Protein expression was then induced by adding 1 mM IPTG and the cells were grown for an additional 4 h at 20°C. The cells were harvested by centrifugation at 6000 × *g*, and the pellet was resuspended in lysis buffer (25 mM Tris/HCl (pH 7.5), 500 mM NaCl, 10 mM imidazole, 0.2% (w/v) Igepal, 2 mM β-mercaptoethanol and 10% (v/v) glycerol) and stored at −80°C. Prior to cell lysis, 277.3 U DNase I (Invitrogen) and one tablet of cOmplete ethylenediaminetetraacetic acid (EDTA)-free protease inhibitor cocktail (Roche Life Science) were added to the cell suspension. The cells were lysed by sonication, and the resulting slurry was clarified by centrifugation at 48 000 × *g*. After filtration using a 0.2 μM syringe filter, the supernatant was mixed with 1 ml Ni-NTA gel (Qiagen), pre-equilibrated with lysis buffer, and incubated under gentle rotation for 1.5 h at 4°C prior to loading onto a gravity flow column. Non-specifically bound proteins were washed out with buffer B (25 mM Tris/HCl (pH 7.5), 500 mM NaCl, 20 mM imidazole, 0.02% (w/v) Igepal and 10% (v/v) glycerol) followed by elution of the target protein with buffer B containing 300 mM imidazole, yielding five 1-ml fractions. Sufficiently pure fractions were pooled and mixed with 0.4 ml anti-FLAG M2 resin (Sigma-Aldrich) pre-equilibrated with FLAG buffer (25 mM Tris (pH 7.5), 500 mM NaCl, 0.02% (w/v) Igepal and 10% (v/v) glycerol) and incubated under slow rotation for 3 h at 4°C. Next, the slurry was transferred to a gravity flow column and washed with 10 ml FLAG buffer. Afterward, 400 μl FLAG buffer containing 0.5 mg/ml FLAG peptide (Sigma-Aldrich) was added to the column and then incubated for 30 min at 4°C before collecting the eluate. This elution procedure was repeated two times. Finally, the pure fractions were pooled together and centrifuged in an Amicon filter unit (Millipore) with a molecular weight cutoff of 10 kDa in order to eliminate co-eluted FLAG peptide, and this was followed by flash-freezing in liquid nitrogen before storage at −80°C. Protein purity and the presence of degradation products were assessed by sodium dodecyl sulphate-polyacrylamide gel electrophoresis (SDS-PAGE) as well as western blotting using anti-His_6 antibodies (GenScript), and the protein concentration was determined by Bradford assay (Roche Life Science).

Electrophoretic mobility shift assay (EMSA) and helicase assay

EMSA was performed in 20 μl reaction mixtures containing 50 mM Tris/HCl (pH 8.5), 2 mM 1,4-dithiothreithol (DTT), 0.25 mg/ml bovine serum albumin, 2 mM $MgAc_2$, 100 mM NaCl/KCl and 4 fmol ^{32}P-labeled DNA (final concentration of 0.2 nM). The oligonucleotides were end-labeled using T4 kinase (ThermoScientific) and γ-ATP at 37°C. The labeled oligonucleotides were purified on 10, 15 or 20% native polyacrylamide gels depending on the type of DNA substrate. The gel and running buffer contained 10 mM NaCl or KCl when the oligonucleotides were folded in

NaCl or KCl. The EMSA reaction was started by addition of protein (final concentration of 0.0096, 0.096, 0.96 or 9.6 nM) and incubated for 10 min at 30°C. The samples were subjected to electrophoresis using a 10% native polyacrylamide gel at 110V for 60 min in 1× Tris/Borate/EDTA (TBE) buffer with either 10 mM NaCl/KCl (G4 DNA) or no salt (single-stranded DNA (ssDNA) and 5′-3′ partial duplex DNA substrate (see Supplementary Table S1)) in the gel and the running buffer. The gel was dried on a 3MM Whatman filter paper, phosphorimaged (Fujifilm) overnight and visualized with a Typhoon 9400 Variable Mode Imager (Amersham Biosciences/GE Healthcare).

The procedure to determine the helicase activity of nPfh1 was similar to the EMSA, with the exception of adding adenosine triphosphate (ATP) to the reaction mixture. When Phen-DC_3 (0.2 or 1 nM final concentration) was used, it was preincubated together with the DNA for 30 min at room temperature before addition of protein. After 10 min incubation at 30°C, the reaction was stopped by adding 4 μl of 6× stop solution (60 mM EDTA (pH 8.0), 40% (w/v) sucrose, 0.6% SDS and 0.25% bromophenol blue) on ice. For the experiments using a cold protein trapping oligonucleotide (75-nt long, see Supplementary Table S1), 0.2 nM rDNA G4 folded in 1 M NaCl was preincubated with 9.6 nM nPfh1 for 5 min at 30°C, followed by reaction initiation using 2 mM ATP ± 4.8 μM trap DNA. Aliquots (10 μl) were then withdrawn at various time points (0 s, 15 s, 30 s, 45 s, 1 min, 3 min, 5 min, 10 min and 15 min), and the reactions were stopped by adding 2 μl of 6× stop solution. To separate intact DNA from unwound product, electrophoresis was performed using a 10% native polyacrylamide gel at 110V for 60 min in 1× TBE buffer with 10 mM NaCl/KCl in both the gel and running buffer, followed by gel drying, phosphorimaging and analysis on the Typhoon imager. For both the EMSA and helicase assay, the gel bands were quantified with the ImageQuant software. To calculate the amount of bound or unwound DNA, the formula [% bound/unwound = 100 × (P/(P + S))] was used, where P is bound or unwound DNA and S is the background-corrected (no protein added) unbound or intact DNA.

ATPase assay

Unless otherwise stated, 2 nM nPfh1 was incubated for 20 min at 30°C in the presence of various oligonucleotides in a buffer containing 50 mM Tris/HCl (pH 8.5), 100 mM NaCl/KCl, 5 mM $MgCl_2$, 2 mM DTT and 2 mM ATP in a reaction volume of 50 μl. A total volume of 100 μl of BIOMOL Green reagent (Enzo Life Sciences) was added to the reaction followed by a 25 min incubation at room temperature before measuring the absorbance at 620 nm using an Infinite M200 plate reader (TECAN). The measurements were performed with the following parameters: 3 s shaking (2 mm amplitude, orbital mode, 57 rpm frequency), 25 flashes and 0 ms settle time. The amount of phosphate released was calculated using a phosphate standard provided in the kit (Enzo Life Sciences) and used according to the manufacturer's instructions.

RESULTS

The predicted G4 sequences in *S. pombe* rDNA and telomeric repeats form G4 structures *in vitro*

To investigate whether the predicted G4 motifs in *S. pombe* form G4 structures, we analyzed the formation of G4 structures using CD spectroscopy. CD spectroscopy is commonly used to study the formation of polymorphic DNA structures, including G4 structures (8,35) and whether the G4 motif adopts a G4 structure as well as what type of G4 structure is formed can be determined from the profile of the spectrum. In this study, we focused on two different G4 motif-enriched regions; rDNA and telomeres (7). G4 structures are stabilized by the presence of cations, such as Na^+ and K^+, and the stability and the structure formed can differ depending on the cation species, the ionic strength and the sequence of the oligonucleotide (1).

Here, we folded the *S. pombe* telomeric and rDNA oligonucleotides (Figure 1A and Supplementary Table S1) using four different cation conditions (100 mM NaCl, 100 mM KCl, 1 M NaCl and 1 M KCl) and analyzed them by CD spectroscopy. Preliminary CD measurements (data not shown) demonstrated that out of the five different G4 motifs in the rDNA region, the G4 motif highlighted in Figure 1B gave rise to the most prominent G4 profile and was therefore selected for further studies. Hereafter, both our *in vitro* and *in vivo* studies are focused on this specific rDNA G4 motif. To determine the thermal stability of the structures, the measurements were performed at four different temperatures (25, 45, 65 and 85°C). When the rDNA oligonucleotide was folded in either 100 mM or 1 M NaCl, it displayed spectra characterized by a negative peak at 245 nm and a positive peak at 264 nm (Figure 1C), which are typical features of a parallel G4 structure (36). As the temperature was raised, the amplitude of the peaks diminished, showing an increased melting of the G4 structure at higher temperatures. More G4 structures were formed in 1 M NaCl as evident by the increase in signal compared to the rDNA oligonucleotide folded in 100 mM NaCl (Figure 1C). Folding in KCl also gave rise to a parallel G4 profile (Figure 1D), and there appeared to be greater G4 formation compared to NaCl. Already at 100 mM KCl, the signal intensity was higher than for 1 M NaCl. In addition, the thermal stability of the G4 structures increased in the presence of KCl because raising the temperature from 25 to 45°C resulted in a much smaller signal reduction compared to the G4 structures formed in the presence of NaCl. In contrast, the telomeric G4 oligonucleotide folded in either 100 mM or 1 M NaCl displayed spectra with very low signal that barely changed when the temperature increased, indicating little formation of G4 structures (Figure 1E). However, folding in KCl greatly enhanced the G4 structure formation of the telomeric oligonucleotide resulting in a predominantly parallel G4 conformation, albeit with a broader peak compared to the rDNA oligonucleotide (Figure 1D and F).

To examine whether random G-rich sequences can form G4 structures, we designed scrambled sequences of the rDNA and telomeric G4 motifs (Supplementary Figure S1A and Supplementary Table S1). These sequences contained the same nucleotide composition as the original

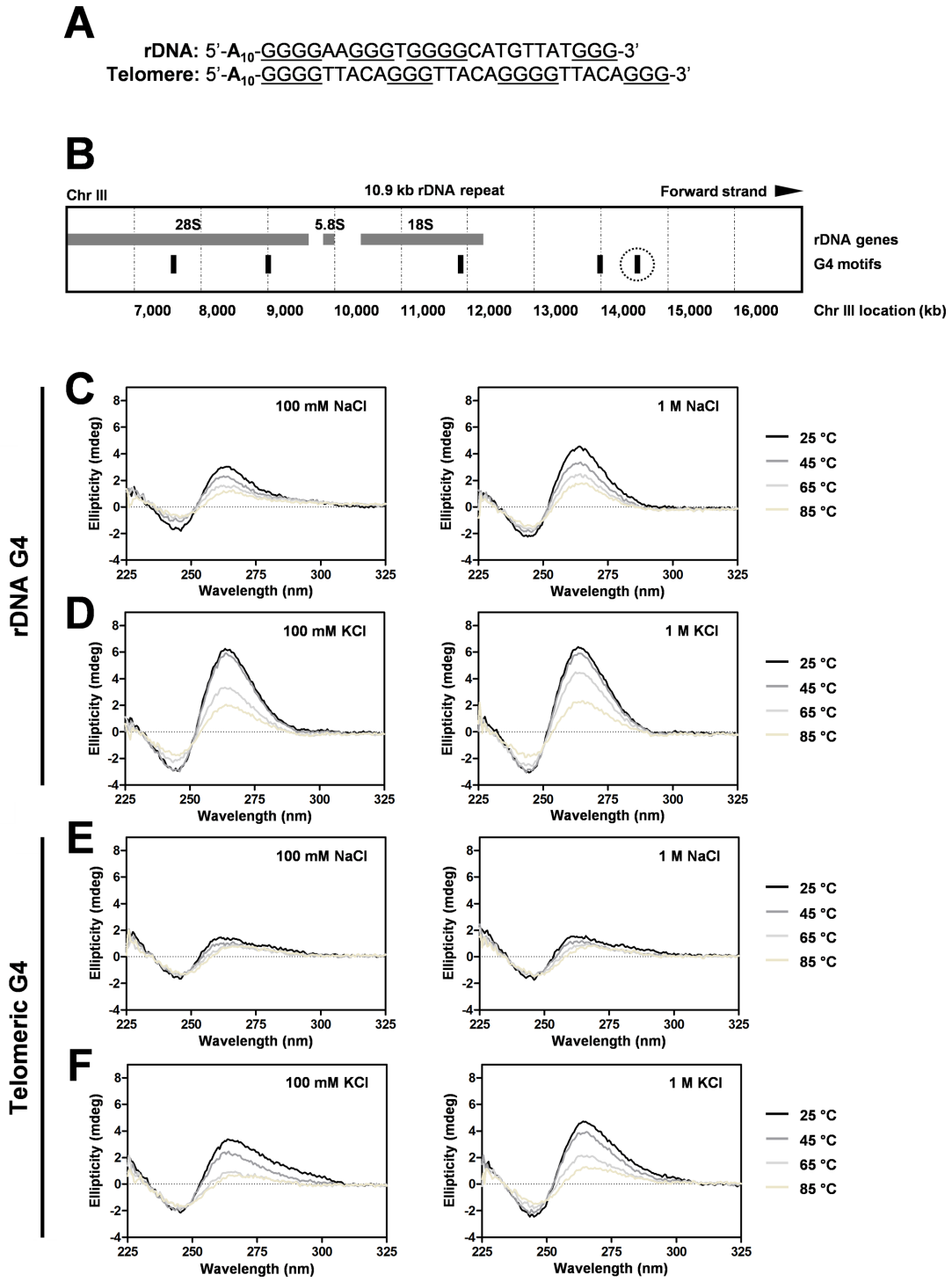

Figure 1. *Schizosaccharomyces pombe* rDNA and telomeric DNA fold into G4 structures *in vitro*. (**A**) Sequences of oligonucleotides with the G4 consensus motifs from *S. pombe* rDNA and telomeric regions. The G-tracts are underlined. A poly$(A)_{10}$ sequence is included in both oligonucleotides and shown in bold. (**B**) Cartoon of an rDNA repeat (10.9 kb) in *S. pombe*, showing the five G4 motifs as black bars and the G4 motif used in this study highlighted by a dotted circle. (**C**) CD spectra recorded for 5 μM rDNA folded in NaCl or (**D**) KCl at different temperatures. The spectra were measured at 225–325 nm at 25, 45, 65 and 85°C. (**E**) CD spectra for 5 μM *S. pombe* telomeric DNA folded in NaCl or (**F**) KCl, measured as in C and D.

oligonucleotides, but the order of the nucleotides was changed. At 25°C, the scrambled rDNA sequence showed a broadened positive peak with a much lower amplitude compared to the wild-type oligonucleotide in both 1 M NaCl and KCl (Supplementary Figure S1B). When the temperature was raised to 85°C the peak disappeared, indicating melting into an unfolded structure. For the scrambled telomeric G4 oligonucleotide the signal intensity of the profile was considerably higher and the positive peak was centered around 275 nm (Supplementary Figure S1C), suggesting that random G-rich sequences can fold into G4 DNA to some extent, but the endogenous G4 motifs are needed in order to form stable G4 structures. Together, these observations indicate that oligonucleotides of *S. pombe* rDNA and telomeric G4 motifs can form G4 structures and that K^+ ions stabilize the rDNA and telomeric G4 structures to a greater extent than Na^+ ions.

rDNA and telomeric G4 structures have different molecularities and are disrupted by mutations in the G-tracts

To further confirm that the rDNA and telomeric oligonucleotides adopt G4 structures *in vitro*, a ThT-based assay was performed. ThT is a fluorescent compound that has the property to emit a higher signal when bound to G4 structures compared to single- or double-stranded DNA (34,37). We found that the fluorescence signal of ThT was significantly higher ($P < 0.05$) for the telomeric and rDNA oligonucleotides folded in salt (NaCl or KCl) compared to the absence of salt (Supplementary Figure S2). In particular, the fluorescence of ThT was largely increased in the presence of the putative G4-forming rDNA oligonucleotide folded in either NaCl or KCl (Figure 2A and Supplementary Figure S2). Consistent with our CD analysis, the telomeric oligonucleotide showed a much higher ThT fluorescence signal when folded in KCl compared to NaCl (Figures 1E, F and 2A; Supplementary Figure S2).

To further validate the formation of G4 structures, mutated rDNA and telomeric oligonucleotides comprising a single substitution of guanine to thymine in one of the G-tracts (rDNA-m1 and telomere-m1) or in each of the four G-tracts (rDNA-m4 and telomere-m4) were examined (Figure 2A). To ensure optimal folding conditions, 1 M KCl was used. We anticipated that mutations in the G-tracts would reduce the stability of the G4 structure and therefore a decrease in ThT fluorescence enhancement would be detected. All of the mutated oligonucleotides (rDNA-m1, rDNA-m4, telomere-m1 and telomere-m4) showed reduced fluorescence enhancement compared to their wild-type counterparts ($P < 0.02$). In particular, rDNA-m4 and telomere-m4 failed to induce any substantial increase in ThT fluorescence signal.

We also analyzed the mutated rDNA and telomeric oligonucleotides by CD spectroscopy at 25, 45, 65 and 85°C. We found that both the rDNA-m1 and the telomere-m1 oligonucleotides were slightly less stable compared to the rDNA and telomeric sequences (left graph in Figure 2B and also in 2C). The CD signal from the rDNA-m4 and telomere-m4 oligonucleotides shifted toward higher wavelengths, and the peak intensity did not change even at 85°C, suggesting that G4 formation was completely disrupted for these oligonucleotides (right graph in Figure 2B and also in 2C). Together, these data strengthen our observations that the putative *S. pombe* rDNA and telomeric G4 sequences can form G4 structures *in vitro*.

To investigate whether the rDNA and telomeric G4 oligonucleotides formed intermolecular or intramolecular G4 structures, the folded oligonucleotides were loaded onto a 10% native polyacrylamide gel to examine their migration patterns. The rDNA G4 oligonucleotide gave rise to higher molecular weight species when treated with 1 M NaCl or 100 mM KCl (left and middle panels in Supplementary Figure S3A), showing that it was able to form intermolecular G4 structures. In contrast, the telomeric DNA was not able to form higher molecular weight structures in NaCl or KCl (left and middle panels in Supplementary Figure S3A). Because the CD and ThT data strongly indicated that the telomeric oligonucleotide adopts a G4 conformation in 100 mM KCl (Figure 1F and Supplementary Figure S2), it was loaded onto a 15% native polyacrylamide gel, which apart from a band corresponding to ssDNA also resulted in the appearance of a faster migrating species (right panel in Supplementary Figure S3A). Intramolecular G4 structures migrate at a similar or faster rate in native polyacrylamide gels compared to ssDNA (38). To test if this was the case for the folded telomeric sequence, melting experiments monitored by CD were carried out to determine the dependence of the melting temperature (T_m) on the strand concentration. The telomeric G4 DNA did not show any significant dependence of T_m on the strand concentration (Supplementary Figure S3B and C), which supports the formation of an intramolecular G4 structure. For the rDNA sequence folded in 100 mM KCl, the T_m increased as a function of strand concentration (Supplementary Figure S3B and C), supporting that the rDNA oligonucleotide forms intermolecular G4 structures.

Pfh1 is enriched at the rDNA G4 motif and telomeres during S phase

Unresolved G4 structures can cause genome instability (39). Specialized helicases, such as members of the Pif1 family helicases, are associated with G4 motifs *in vivo* and they efficiently unwind G4 structures *in vitro* (17,20,30,40–41). Pfh1 binds telomeres (42), and we asked if Pfh1 is also enriched at the putative G4 motif in rDNA by performing ChIP-qPCR. Our earlier ChIP experiments combined with whole genome sequencing (ChIP-seq) did not detect Pfh1 occupancy at any of the five rDNA G4 motifs (7). We therefore tested if we could detect Pfh1 association with the more sensitive ChIP-qPCR analysis. In these experiments, we used an *S. pombe* strain expressing an epitope-tagged Pfh1 (Pfh1-13Myc) and an untagged control strain (Supplementary Table S3) and performed ChIP in asynchronous cell cultures. Pfh1-13Myc is inserted in the *leu1*$^+$ locus under the control of the endogenous promoter of *pfh1*$^+$, and this strain does not show any significant growth defects compared to wild-type strains with untagged Pfh1 (21). The anti-Myc antibody was used to immunoprecipitate the DNA that was bound by the Pfh1-13Myc protein. We tested Pfh1 occupancy at three different sites—*gal1*$^+$, telomeres using primers binding to subtelomeres and the G4 motif in rDNA

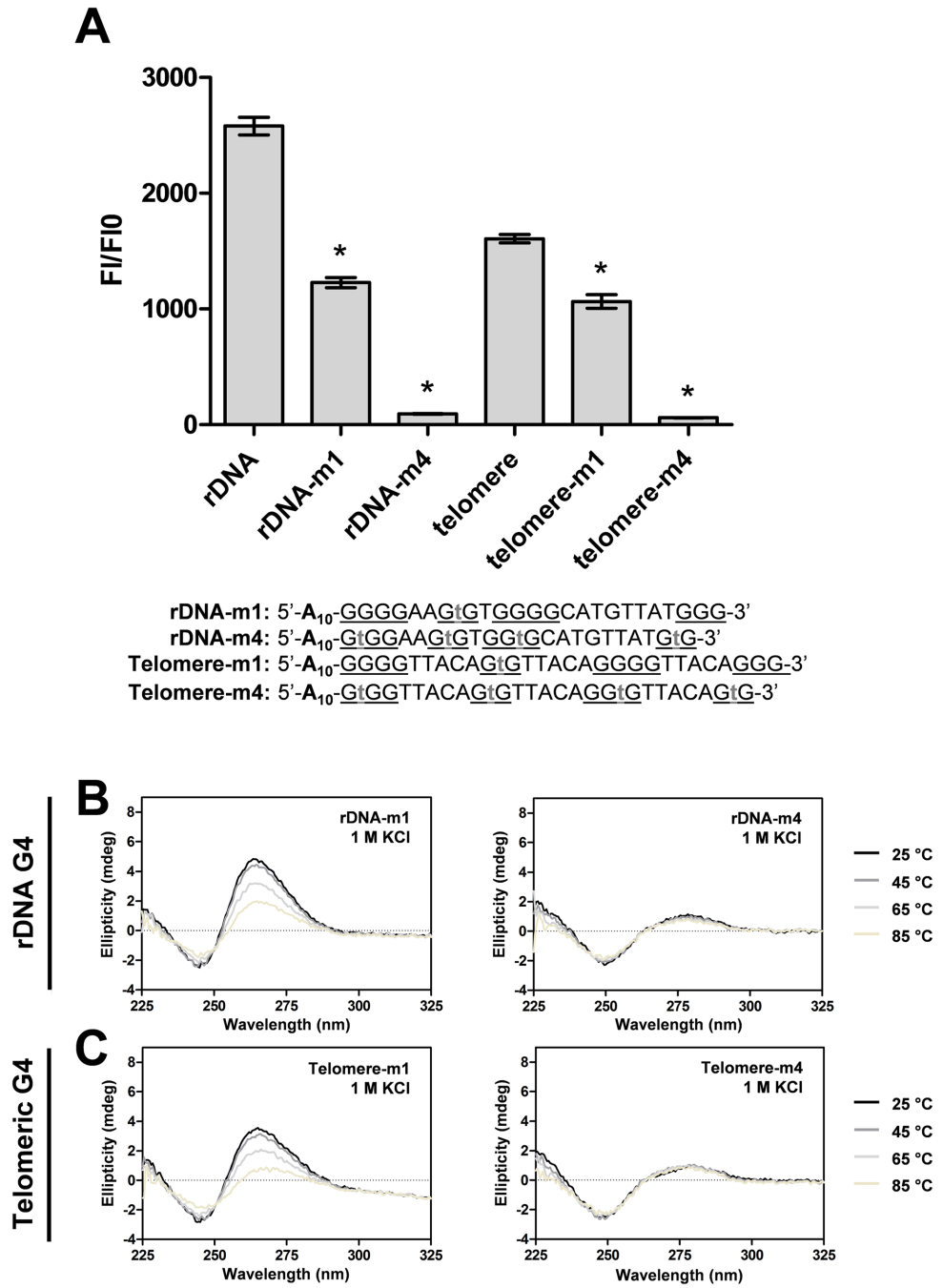

Figure 2. Mutations in the G-tracts of rDNA and telomeric G4 DNA oligonucleotides inhibit the formation of G4 structures. (**A**) Enhancement of ThT fluorescence by wild-type and mutated rDNA and telomeric G4 oligonucleotides folded in 1 M KCl. The data are presented as the ratio of the fluorescence intensity of ThT in the presence of oligonucleotide (FI), divided by the fluorescence intensity of ThT in the absence of oligonucleotide (FI0) after subtracting the fluorescence intensity of buffer only. The data are shown as the average of three samples. Error bars represent the standard deviation, and significant differences ($P < 0.02$) in fluorescence signal as calculated by a two-tailed Student's *t*-test are denoted by * (top). The mutated oligonucleotides contained either a substitution in a single G-tract or a substitution in each G-tract as indicated by a gray letter 't' in the sequences (bottom). (**B**) CD spectra recorded at different temperatures for 5 μM rDNA oligonucleotide bearing a mutation in a single G-tract (rDNA-m1) or a mutation in each G-tract (rDNA-m4). The oligonucleotides were folded in 1 M KCl and measured at 25, 45, 65 and 85°C between 225 and 325 nm. (**C**) CD profiles of the telomeric oligonucleotide with a single mutation in one G-tract (telomere-m1) or a mutation in each G-tract (telomere-m4) folded and measured as in B.

(rDNA G4) (Figure 3A). To assess protein-enrichment at telomeres, primers binding to the subtelomeres adjacent to the telomeres were used (42–44), because primers binding directly to the telomeres yield smeary PCR products due to the repetitive nature of the telomeric regions. Hereafter, this site is called telomeres. Pfh1 binds both Pfh1-dependent and Pfh1-independent DNA sequences, however, sites that are dependent on Pfh1 have higher binding than sites that are not (21). Telomeres have high Pfh1-binding and together they constitute a Pfh1-dependent site because replication through this site is facilitated by the helicase (42). *gal1*$^+$ was used as a control for Pfh1-independent sites because replication through the *gal1*$^+$ gene is not dependent on Pfh1, although it is bound by the protein (21). Pfh1-13Myc had significantly higher binding to all these three sites compared to the untagged control strain ($P < 0.004$), and as previously shown (42) the level of binding was highest for the telomeric sites and lowest for *gal1*$^+$(Supplementary Figure S4A), which is consistent with these being Pfh1-dependent and Pfh1-independent sites, respectively. Binding to the G4 motif at rDNA was lower than to telomeres, but significantly higher than to the *gal1*$^+$ gene (Supplementary Figure S4A), which suggests that the rDNA G4 site may also be a Pfh1-dependent site.

G4 structures are suggested to fold when DNA is single-stranded, perhaps when double-stranded DNA becomes unwound during the DNA replication process. In *S. pombe*, G2 is the longest phase in the cell cycle and thus ∼75% of cells in an exponentially growing asynchronous culture are in G2 phase (13). To further elucidate if the rDNA G4 is a Pfh1-dependent site, we tested if Pfh1 is enriched at rDNA G4 outside G2 phase. If binding of Pfh1 to the tested sites is higher outside of G2 phase, we expect to find similar or higher levels of Pfh1-binding in asynchronous cells compared to G2-arrested cells. To arrest the cells in G2 phase, we used a temperature sensitive *cdc25-22* strain expressing Pfh1-13Myc and incubated the cells at the non-permissive temperature (36°C) for 5 h. Binding of Pfh1 to rDNA G4 and telomeres decreased three to 4-fold in G2-arrested cells compared to the asynchronous cells ($P < 0.02$) (Figure 3B). However, the Pfh1-independent *gal1*$^+$site showed no significant difference in Pfh1-enrichment between G2-arrested and asynchronous cells. These data suggest that Pfh1 is enriched at rDNA G4 and telomeres outside of G2 phase, perhaps during S phase when DNA is replicated. To examine if the enrichment occurs during S phase, we again used the Pfh1-13Myc *cdc25-22* strain and arrested the cells in G2 phase at 36°C. By shifting the culture from 36 to 25°C, the cells were released from the arrest and samples were taken for ChIP and FACS analysis throughout a cell cycle (Supplementary Figure S4B and Figure 3C). Next, we monitored Pfh1 association at *gal1*$^+$ site, rDNA G4 and telomeres at all collected time points. Pfh1 was enriched at *gal1*$^+$, rDNA G4, telomeres during mid S phase, mid to late S phase and mid to late S phase, respectively (Figure 3C).

Purified nPfh1 helicase binds to *S. pombe* rDNA and telomere G4 DNA *in vitro*

In order to examine if Pfh1 directly binds rDNA and telomeric G4 DNA, Pfh1 was overexpressed and purified. The *pfh1*$^+$ gene consists of two translational start sites (Figure 4A) (29). The first AUG encodes a mitochondrial isoform of Pfh1, whereas the second AUG gives rise to a nuclear isoform (29). We cloned the nuclear isoform of Pfh1, and to improve the expression, solubility and purification of protein, several epitope tags were tested in *Escherichia coli*. His_6-Trx-nPfh1-FLAG (simply referred to as nPfh1) was chosen as the best candidate because using Trx as a carrier protein provided the highest expression level of soluble protein and the His_6- and FLAG-tags enabled purification to homogeneity. As a control for potential helicase activities of any remaining contaminating proteins, an ATPase-inactive variant, nPfh1-K338A with a lysine mutated to alanine in the Walker A box (Figure 4A), was expressed and purified in parallel. SDS-PAGE and western blot of the two proteins showed negligible amounts of contaminating proteins or degradation products (Figure 4B and C).

The CD experiments demonstrated that 1 M NaCl stabilized the G4 structures more efficiently than 100 mM NaCl, while for KCl the physiologically more relevant concentration of 100 mM (45,46) appeared to be sufficient for stabilizing the G4 structure. Therefore, the rDNA and telomeric oligonucleotides were folded in either 1 M NaCl or 100 mM KCl, followed by extraction of the bands corresponding to the G4 structures from the gel (Supplementary Figure S3A). First, the G4 DNA-binding properties of nPfh1 and nPfh1-K338A were examined by EMSA, using protein concentrations from 9.6 pM to 9.6 nM and a constant ^{32}P end-labeled DNA concentration of 0.2 nM for all samples. Wild-type nPfh1 bound with high affinity to the rDNA oligonucleotide folded in either NaCl or KCl (Figure 5). Approximately 60% of the DNA was bound in the reaction in which 5-fold excess of protein to DNA was added (lane 4 in Figure 5A and also in 5B), and a full shift was reached at the highest protein concentration (lane 5 in Figure 5A and also in 5B). nPfh1-K338A displayed a lower binding capacity for the rDNA sequence folded in NaCl, but not when it was folded in KCl (lanes 6–9 in Figure 5A and also in 5B). Also, wild-type nPfh1 exhibited little binding to the telomeric G4 DNA folded in KCl (lanes 2–5 in Figure 5C), and the binding of nPfh1-K338A was completely abolished (lanes 6–9 in Figure 5C).

ScPif1 binds to G4 DNA better than to ssDNA (47), and to test whether this was also the case for nPfh1, EMSA was performed with a 10 nt poly(A) oligonucleotide that corresponded to the $poly(A)_{10}$ tail of the G4 oligonucleotides. Similar to ScPif1 (47), the nPfh1 proteins were unable to induce a shift of the labeled DNA, suggesting that nPfh1 was not able to bind to the short stretch of adenines alone (Supplementary Figure S5A). Next, we asked whether nPfh1 bound any DNA substrates when the short ssDNA overhang was conjugated to a secondary DNA structure, similar to the folded G4 oligonucleotides. Thus, binding to a 5′-3′ partial duplex with a $poly(A)_{10}$ overhang was analyzed. Both the wild-type and mutated proteins were unable to bind tightly to the partial duplex DNA substrate (Supplementary Figure S5B), indicating that the presence of a G4 structure can slightly stimulate the binding of nPfh1 to a DNA substrate

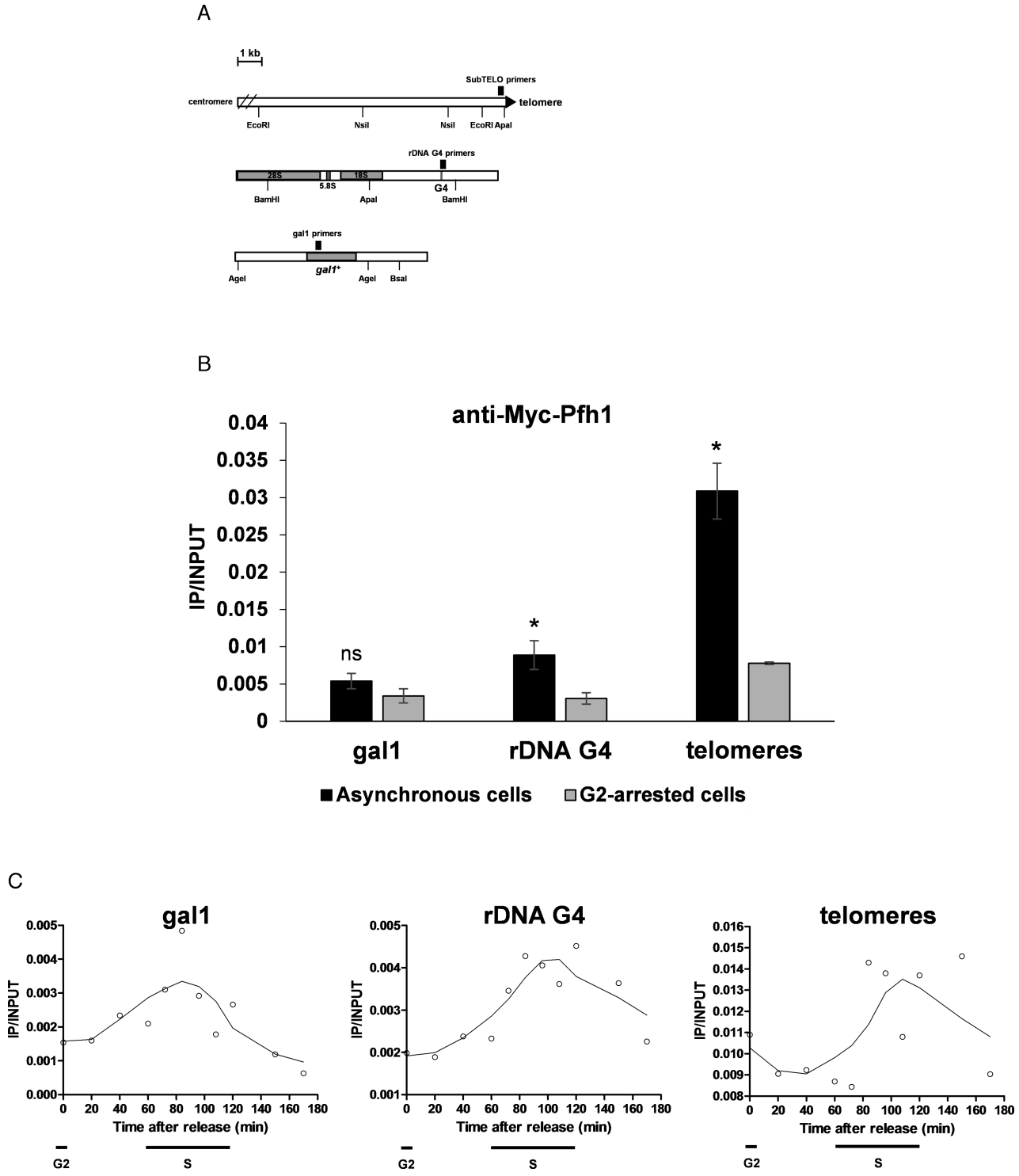

Figure 3. Pfh1 is enriched at rDNA and telomeres during S phase. (**A**) Schematics indicating the position of the primer pairs used for qPCR as well as of restriction sites. The primer products are shown as black boxes, telomere as a black triangle and the position of the studied G4 motif in an rDNA repeat is indicated as a gray line. (**B**) Samples from asynchronous or G2-arrested cells expressing Pfh1-13Myc grown in YES media were chromatin immunoprecipitated using an anti-Myc antibody. The immunoprecipitated DNA was analyzed using qPCR with primers specific for three regions—*gal1*$^{+}$, rDNA G4 and telomeres. Pfh1 association is shown as immunoprecipitated DNA divided by input DNA. Data represent the mean of three independent replicates. Error bars show the standard deviations. The *P*-value ($P < 0.02$) was determined by a two-tailed Student's *t*-test. *, significant difference between asynchronous cells and G2-arrested cells; ns, not significant. (**C**) Samples from different time points throughout a cell cycle were collected and immunoprecipitated using anti-Myc antibody and analyzed as in A. Each open circle represents the immunoprecipitated DNA divided by input DNA. The smoothed graph line is drawn using GraphPad Prism software. G2 and S phases are indicated below each graph.

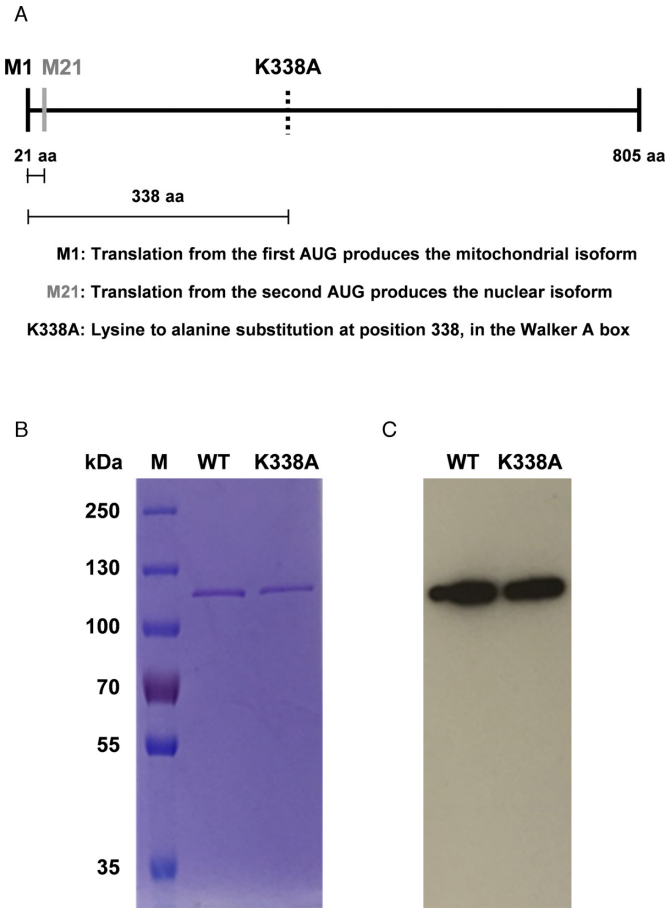

Figure 4. Purification of nPfh1. (**A**) Schematic of the protein encoded by the *pfh1*$^+$ gene. When the first starting Met (M1) is utilized during translation, Pfh1 is translocated to the mitochondria by a targeting signal peptide, which is subsequently cleaved. In contrast, translation from the second Met (M21) leads to the production of the nuclear isoform. Substitution of a lysine with an alanine at position 338 (denoted K338A), located in the nucleotide-binding Walker A box, renders a helicase-inactive Pfh1. (**B**) Coomassie Blue stained SDS-PAGE gel and (**C**) western blotting of purified wild-type nPfh1 (WT) and helicase-inactive nPfh1-K338A (K338A). M denotes the DNA ladder. Anti-His_6 antibodies were used for western blot detection.

Finally, the binding of nPfh1 to non-folded G4 oligonucleotides (no salt was added to the oligonucleotides) was investigated to determine whether the high affinity to the rDNA G4 structure was due to its conformation and not due to sequence of the oligonucleotide *per se*. In contrast to the poly(A) and 5′-3′ partial duplex DNA substrates, nPfh1 was able to bind both the non-folded rDNA and telomeric oligonucleotides. Although the presence of salt had an inhibitory effect on the binding properties of nPfh1 (data not shown), binding to the non-folded rDNA oligonucleotide at the highest protein concentration was slightly lower compared to nPfh1 binding to the folded rDNA oligonucleotide (Supplementary Figure S5C, and Figure 5A and B), and a complete shift was not observed. However, nPfh1 showed a much higher binding affinity to the non-folded telomeric oligonucleotide compared to the folded intramolecular telomeric G4 substrate (Supplementary Figure S5C and Figure 5C). Thus, *in vitro* nPfh1 preferentially binds to the rDNA G4 structure compared to the telomeric G4 structure.

nPfh1 unwinds *S. pombe* rDNA and telomeric G4 DNA *in vitro*

To determine whether nPfh1 is able to unwind stable G4 structures, we examined the helicase activity of the protein using the same protein and DNA concentrations as for the EMSA. We first confirmed that similar to full-length Pfh1 (Pfh1 expressed from the first start codon), nPfh1 had the same 5′ to 3′ polarity (data not shown) (31). Also as predicted, the helicase dead nPfh1-K338A showed no unwinding activity (Supplementary Figure S6), confirming that the observed helicase activity was due to nPfh1 and not to any impurities from the protein purification. Next, the ability of nPfh1 to unwind G4 structures was examined. The recombinant protein was able to efficiently unwind the rDNA G4 structure folded in NaCl (lanes 2–5 in Figure 6A), and maximum unwinding was reached already at a two-fold lower protein to DNA ratio (lane 3 in Figure 6A). nPfh1 also resolved the more stable rDNA G4 structure folded in KCl, but to a much lower extent compared to the rDNA G4 structure folded in NaCl (lanes 7–10 in Figure 6A and B).

Because the telomeric intramolecular G4 structure migrates faster than the unfolded G4 structure, resolution of an intramolecular G4 structure will show a shift to a slower migrating band compared to a folded telomeric G4 structure. The slower migrating band was detected when a 2-fold lower protein concentration compared to DNA was added to the reaction (lane 13 in Figure 6A). nPfh1 unwound the intramolecular telomeric G4 structure more efficiently than the intermolecular rDNA G4 structure folded in KCl (Figure 6A and B), and the unwinding efficiency was similar to the 5′-3′ partial duplex DNA substrate (lanes 16–20 in Figure 6A and B). To confirm that the unwound products corresponded to the fully unfolded oligonucleotides, native polyacrylamide gels loaded with boiled, non-boiled, unwound and non-folded G4 oligonucleotides were run for all three G4 species (Supplementary Figure S7).

To further investigate the G4 resolving activity of nPfh1, the unwinding efficiency was measured in the presence of a protein-trapping cold oligonucleotide. nPfh1 was preincubated with the rDNA G4 folded in NaCl and unwinding reactions were initiated by ATP ± trap DNA, followed by collection of samples at various time points (Figure 7A). Although the rate of unwinding was lower in the presence of the trap DNA, nPfh1 was still able to resolve the G4 substrate (Figure 7B).

Phen-DC_3 stabilizes the rDNA and telomeric G4 structures and induces an antiparallel G4 conformation of the telomeric G4 structure

G4-stabilizing compounds have emerged as potential therapeutic tools to downregulate the transcription of genes involved in tumor formation (48,49). The well-studied bisquinolinium compound Phen-DC_3 is very potent and stabilizes G4 structures of various sequences both *in vitro* and *in vivo* (50–52). To examine the potential G4-stabilizing effect of Phen-DC_3 on the *S. pombe* rDNA and telomeric

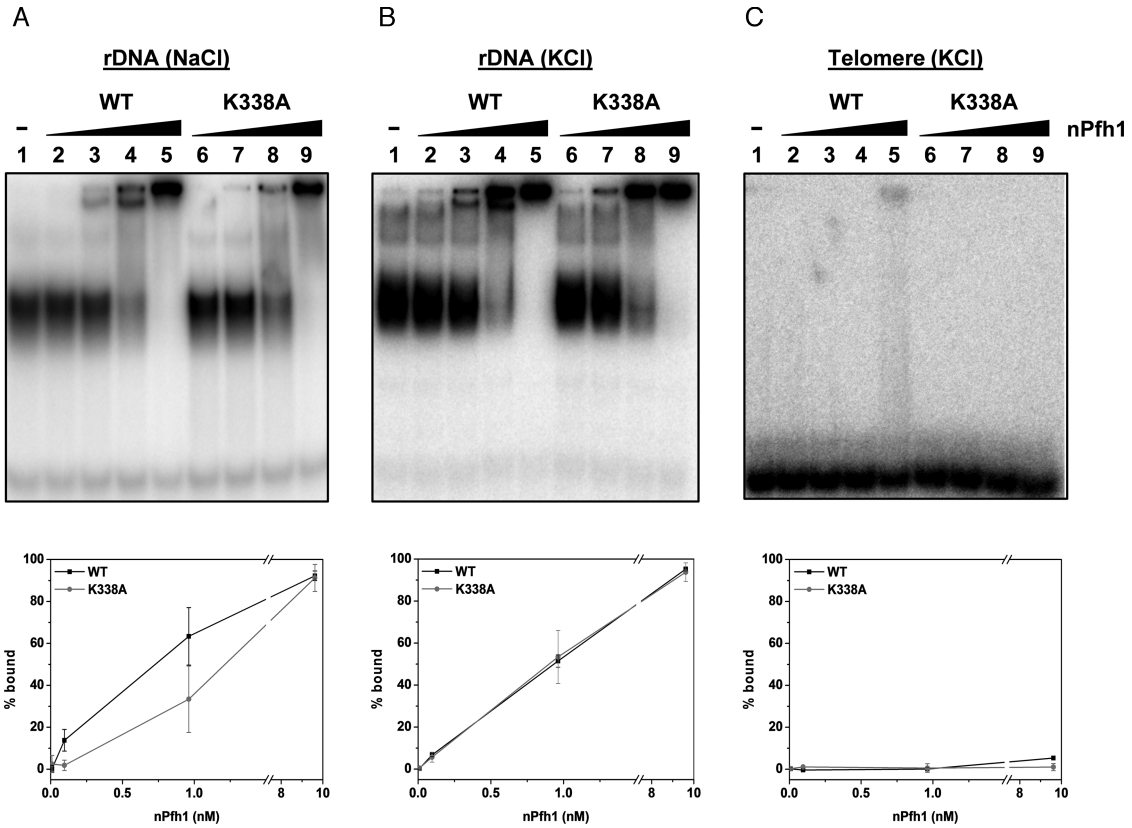

Figure 5. The presence of a G4 structure elicits a higher DNA-binding affinity by nPfh1. EMSA was performed on (**A**) 0.2 nM ^{32}P-labeled rDNA oligonucleotide folded in 1 M NaCl or (**B**) 100 mM KCl and (**C**) the telomeric sequence folded in 100 mM KCl in the presence of 0.0096, 0.096, 0.96 or 9.6 nM nPfh1 (top). Lane 1 contains DNA with no protein. The samples were incubated for 10 min at 30°C and analyzed on 10% native polyacrylamide gels. For each G4 substrate, the assay was performed three times and the amount of protein bound DNA was quantified and averaged (bottom). Error bars represent the standard deviations.

G4 structures, CD experiments were performed in the presence of five-fold higher concentrations of Phen-DC$_3$ over DNA. Phen-DC$_3$ increased the resistance against heat denaturation for both the rDNA and telomeric G4 oligonucleotides folded in 1 M KCl (Figure 8). The rDNA G4 structure remained stable even at 85°C, and only a slight reduction in intensity of the CD signal was detected (left graph in Figure 8A). However, at 25°C the peak intensity was slightly reduced but broadened compared to the CD spectrum of the untreated rDNA G4 substrate at the same temperature (right graph in Figure 1D and left graph in Figure 8A).

At 25°C, the profile of the CD spectrum of the telomeric G4 DNA was even broader in the presence of Phen-DC$_3$, indicating a hybrid G4 formation or a mixed population of parallel and antiparallel G4 conformations (left graph in Figure 8B). At 85°C, the peak shifted to higher wavelengths, suggesting a change to a predominantly antiparallel G4 structure. Similar patterns were observed for both wild-type G4 oligonucleotides folded at a physiologically more relevant KCl concentration (100 mM) compared to 1 M KCl (Supplementary Figure S8). When the oligonucleotides were folded in 100 mM KCl, Phen-DC$_3$ appeared to have even more pronounced effects on the G4 structures; the rDNA G4 structure was even more thermally stable and the telomeric G4 structure was further shifted toward the antiparallel conformation.

Despite bearing a mutation in one of the G-tracts, rDNA-m1 and telomere-m1 still retained the ability to form G4 structures (left graph in Figure 2B and also in 2C). Therefore, we tested whether Phen-DC$_3$ was able to stabilize these structures as well. Indeed, Phen-DC$_3$ stabilized both rDNA-m1 and telomere-m1 (middle graph in Figure 8A and also in 8B). Also, we found that Phen-DC$_3$ was able to induce the formation of the tested G4 structures. This was most apparent for the rDNA-m4 G4 oligonucleotide, which in the absence of Phen-DC$_3$ displayed a random coil-like CD profile but upon addition of Phen-DC$_3$ acquired a G4 structure that could be denatured (right graph in Figure 8A). For telomere-m4, Phen-DC$_3$ slightly induced the formation of G4 structures that disappeared at higher temperatures (right graph in Figure 8B). Together, these data demonstrate that Phen-DC$_3$ can stabilize both *S. pombe* rDNA and telomeric G4 structures and induce the formation of G4 structures in G-rich sequences.

nPfh1 unwinds Phen-DC$_3$-stabilized G4 structures

As inferred from the CD data, the G4 structures were considerably more stable in the presence of Phen-DC$_3$. To investigate whether nPfh1 had the ability to unwind Phen-DC$_3$-stabilized G4 structures, helicase assays were performed with the rDNA and telomeric G4 oligonucleotides treated

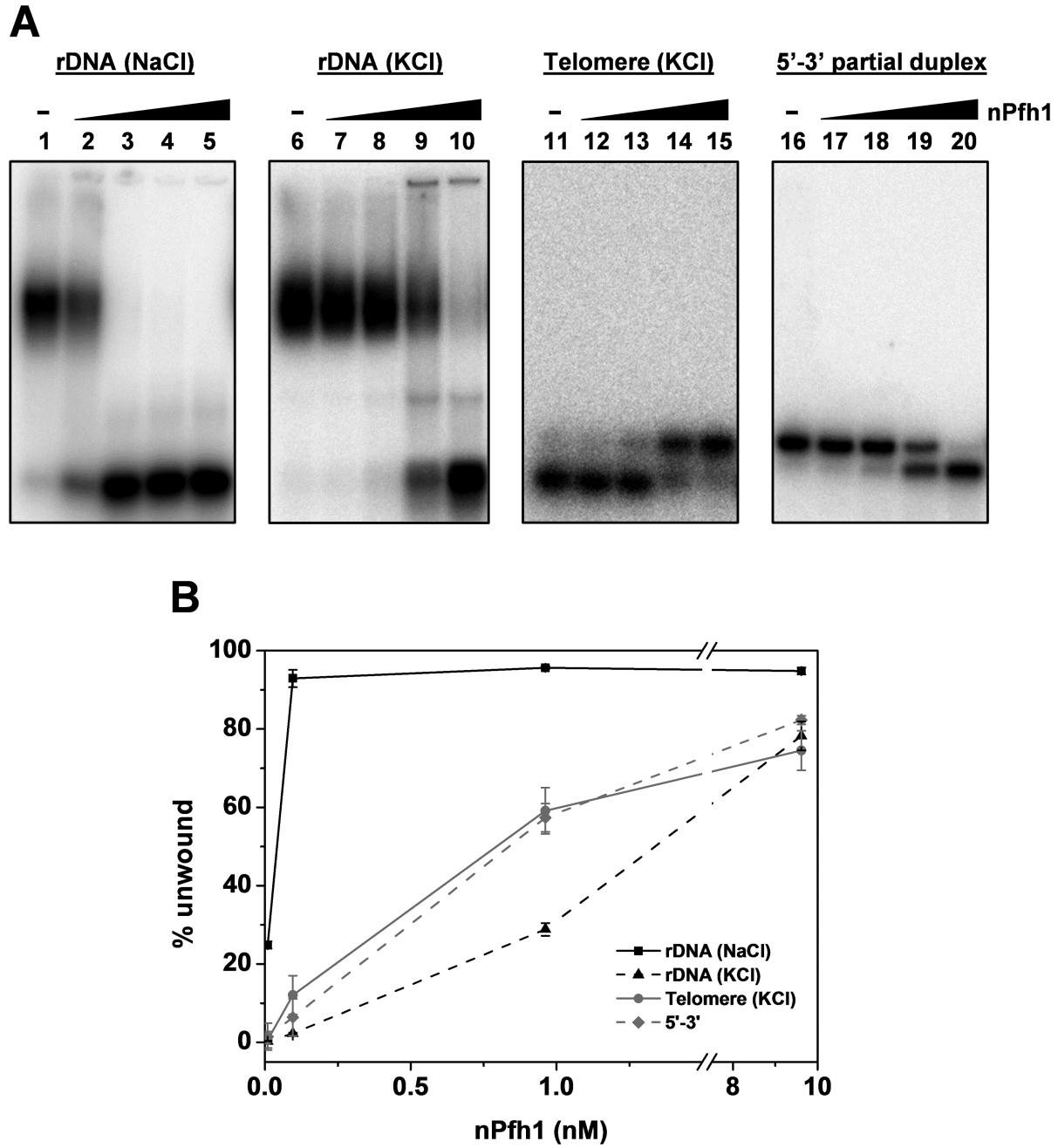

Figure 6. nPfh1 unwinds G4 substrates. (**A**) 0.2 nM ^{32}P-labeled rDNA sequence folded in 1 M NaCl (lanes 1–5) or in 100 mM KCl (lanes 6–10), the telomeric oligonucleotide folded in 100 mM KCl (lanes 11–15) and a partial duplex DNA with a poly(A)$_{10}$ overhang (lanes 16–20; also shown in Supplementary Figure S6) were treated with 0.0096, 0.096, 0.96 or 9.6 nM nPfh1 and analyzed on 10% native polyacrylamide gels. The lanes labeled '–' have DNA in the absence of protein. (**B**) For each DNA substrate, the assay was performed three times and the amount of unwound product was quantified. The average amount of unwound DNA is shown and error bars represent the standard deviations.

with either 0.2 or 1 nM Phen-DC$_3$ (1:1 or 1:5 DNA:Phen-DC$_3$ molar ratio, respectively). In the presence of 0.2 nM Phen-DC$_3$, nPfh1 unwound the rDNA folded in NaCl as efficiently as in the absence of the compound. However, in the presence of 1 nM Phen-DC$_3$, a slight inhibition of nPfh1's helicase activity was detected (Figure 9A). Surprisingly, even at 1 nM of Phen-DC$_3$ there was no significant increase in the resistance to unwinding of the rDNA G4 structure folded in KCl (Figure 9B), which displayed the same level of unwound products as in the absence of the compound (Figure 6B). This suggests that although the thermal resistance of the rDNA G4 structure folded in KCl was increased in the presence of Phen-DC$_3$ (compare left graph in Figure 1D and left graph in Supplementary Figure S8), nPfh1 could still resolve the G4 structure efficiently.

We also treated the telomeric G4 structure with Phen-DC$_3$, which resulted in a substantial reduction in the amount of unwound products (Figure 9C). At 0.2 nM Phen-

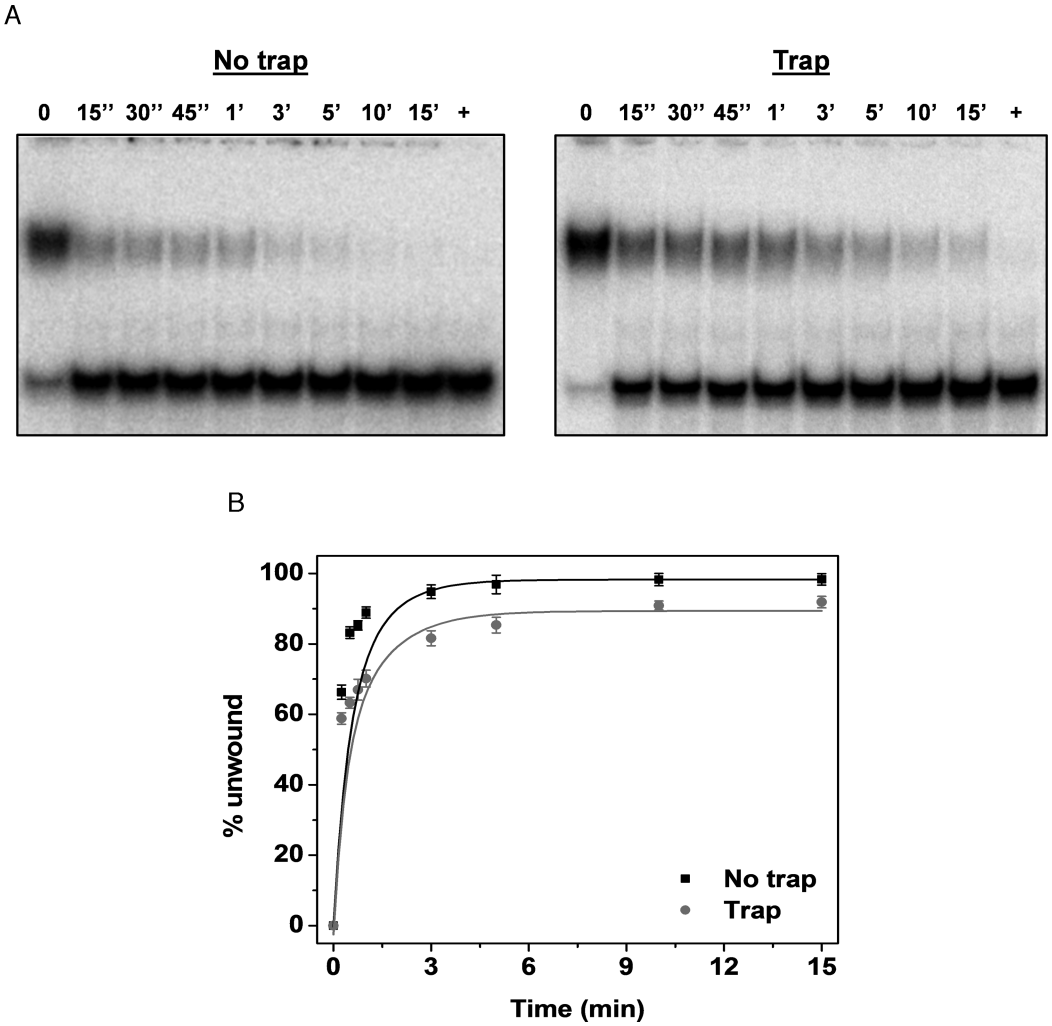

Figure 7. nPfh1 unwinds G4 structures in the presence of trap DNA. (**A**) Unwinding of 0.2 nM ^{32}P-labeled rDNA G4 folded in 1 M NaCl by 9.6 nM nPfh1, in the absence (left) and the presence (right) of 4.8 μM trap DNA. Following a 5 min preincubation at 30°C, the reactions were initiated by adding 2 mM ATP +/− trap DNA and 10 μl aliquots were withdrawn at 0 s, 15 s, 30 s, 45 s, 1 min, 3 min, 5 min, 10 min and 15 min. '+' indicates boiled substrate. (**B**) Quantification of the amount of DNA unwound by nPfh1 as a function of time. Mean values of three replicates are shown, and error bars represent the standard deviations.

DC_3, the amount of unwound product was reduced to ∼50% (Figures 6B and 9C), and at 1 nM Phen-DC_3 ∼30% of the substrate was unwound compared to about 80% in the untreated samples (Figures 6B and 9C).

To rule out the possibility that the inhibition of G4 unwinding was due to an inhibitory effect of Phen-DC_3 on nPfh1 and not to an increase in G4 structure stability, the 5′-3′ partial duplex DNA substrate was tested in helicase assays in the presence of 0.2 and 1 nM Phen-DC_3. Unwinding of the partial duplex substrate by nPfh1 was not inhibited by the Phen-DC_3 treatment (Figure 6B and Supplementary Figure S9), thus the observed reduction in the amount of unwound G4 substrate was due to the stabilizing effect of Phen-DC_3 on the G4 structures.

The presence of G4 structures strongly inhibits the ATPase activity of nPfh1

The ATPase activity of nPfh1 was measured by using the BIOMOL Green reagent assay that quantifies the amount of free phosphate released by the protein. ATP hydrolysis was first measured using 5 nM folded rDNA G4 oligonucleotide or a single-stranded 57 nt non-G4 oligonucleotide in the presence of 1, 2 or 10 nM nPfh1 (Figure 10A). In reactions where 5-fold less nPfh1 (1 nM) than DNA was used, the level of hydrolyzed ATP with the rDNA G4 structure was 5-fold lower than with the 57-nt non-G4 oligonucleotide. This suggests that nPfh1's ATP hydrolysis and presumably also its translocation on DNA were strongly inhibited by the presence of the G4 structure, whereas an oligonucleotide devoid of G4 structures provided a template which nPfh1 could freely translocate on. The difference in the amount of hydrolyzed ATP was not due to the different lengths of the substrates because the level of hydrolyzed ATP by nPfh1 was similar or even slightly higher for non-G4 forming rDNA-m4 (35 nt) compared to the 57-nt non-G4 oligonucleotide (Figure 10A), but was probably due to the folded G4 structure. Incubation of 2 nM nPfh1 with the substrates significantly increased the level of hy-

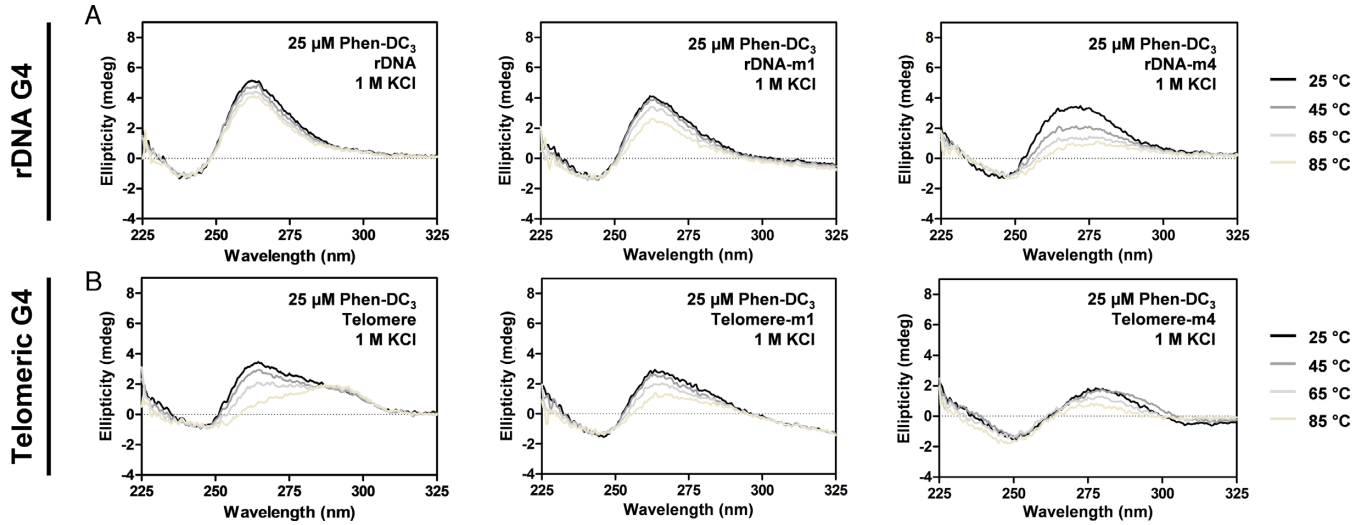

Figure 8. The G4-binding compound Phen-DC_3 stabilizes the *Schizosaccharomyces pombe* rDNA and telomeric G4 structures *in vitro*. (**A**) CD spectra of 5 μM wild-type (left) or mutated (middle and right) rDNA oligonucleotides folded in 1 M KCl and treated with 25 μM Phen-DC_3. Measurements were done at 25, 45, 65 and 85°C. (**B**) Spectra of 5 μM wild-type (left) and mutated telomeric oligonucleotides (middle and right) measured as in A.

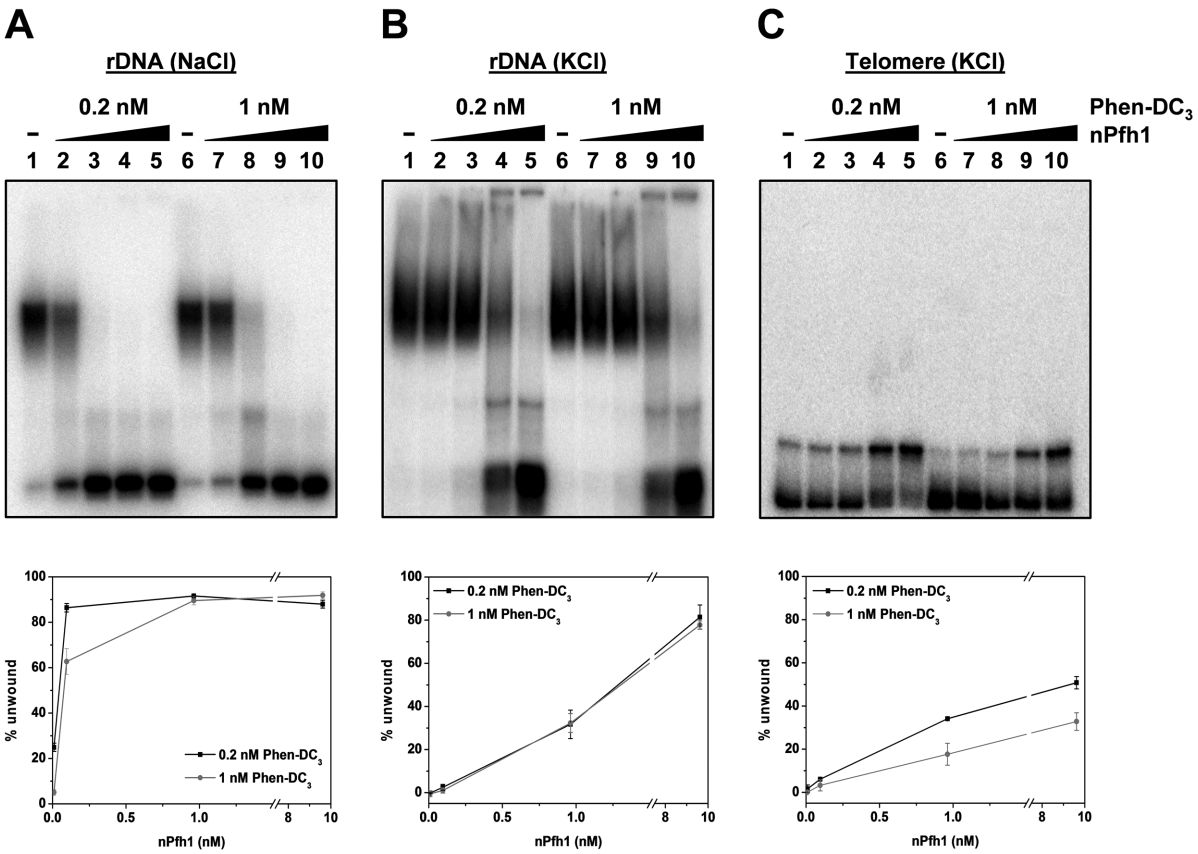

Figure 9. Unwinding of Phen-DC_3–stabilized G4 structures by nPfh1 is slightly reduced. (**A**) 0.2 or 1 nM Phen-DC_3 was preincubated with 0.2 nM ^{32}P-labeled rDNA folded in 1 M NaCl or (**B**) 100 mM KCl, and (**C**) the telomeric sequence folded in 100 mM KCl**.** All of the G4 oligonucleotides were treated with 0.0096, 0.096, 0.96 or 9.6 nM nPfh1, incubated for 10 min at 30°C and analyzed on 10% native polyacrylamide gels (top). The '–' symbol denotes samples without addition of protein. The assay was performed three times for each G4 substrate, and the amount of unwound product was quantified and averaged (bottom). Error bars represent the standard deviations.

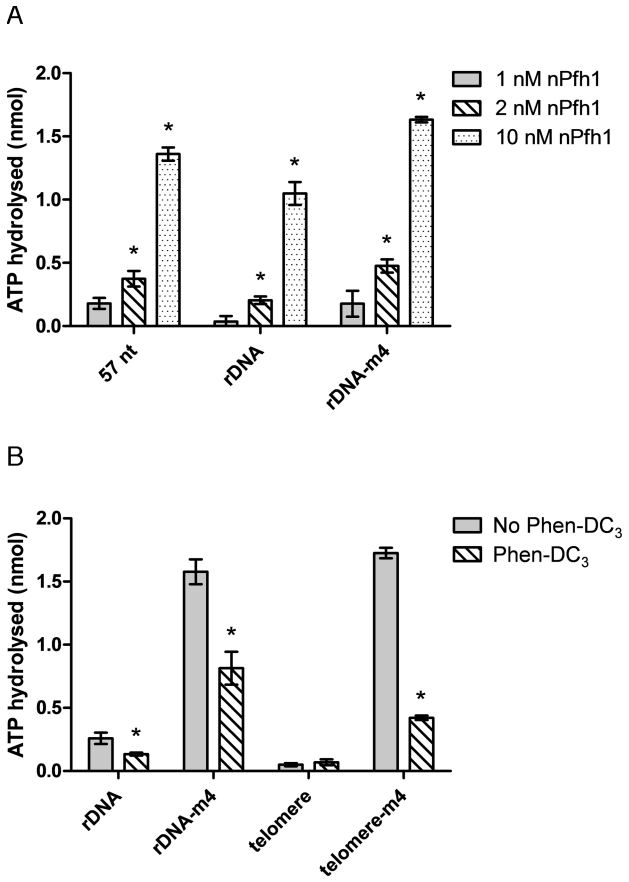

Figure 10. The presence of G4 structures lowers the ATPase activity of nPfh1. (**A**) Measurements of the amount of ATP hydrolyzed by 1, 2 or 10 nM nPfh1 after 10 min incubation in the presence of 5 nM single-stranded oligonucleotide (57 nt), rDNA or rDNA-m4 folded in 100 mM NaCl. (**B**) The amount of ATP hydrolyzed by 2 nM nPfh1 after 20 min incubation the presence of 100 nM rDNA, rDNA-m4, telomere or telomere-m4 oligonucleotides folded in 1 M KCl, in the absence or presence of 500 nM Phen-DC_3. Data in A and B are shown as the average of three samples and error bars represent standard deviations. Significant differences ($P < 0.04$) in ATP hydrolysis between 1 and 2 nM as well as 2 and 10 nM nPfh1 (in A) or the absence or presence of Phen-DC_3 (in B) were calculated by a two-tailed Student's *t*-test and are denoted by *.

drolyzed ATP for all three substrates ($P < 0.04$), demonstrating that higher amounts of nPfh1 increased the ATP hydrolysis. Based on our helicase assay (lane 3 in Figure 6A), the majority of the G4 structures should be unwound at this 2.5:1 DNA:protein molar ratio. Using 2-fold more protein (10 nM) than DNA again led to a significant increase in the ATPase activity of the protein on all three substrates ($P < 0.04$), and showed that the level of ATP hydrolyzed for the rDNA G4 substrate was only slightly lower than for the single-stranded non-G4 substrate. These results indicate that after complete or nearly complete unwinding of the G4 structure by nPfh1, the helicase translocated along the rDNA substrate in a similar way as on the non-G4 ssDNA and thus kept the rDNA G4 structure unfolded.

To determine whether stable G4 structures impair the ATPase activity of nPfh1, ATP hydrolysis by nPfh1 was analyzed in more detail using an even lower protein concentration (1:50 protein:DNA molar ratio) in the presence or absence of Phen-DC_3. ATP hydrolysis by nPfh1 was 4-fold higher for the 57-nt single-stranded oligonucleotide and rDNA-m4 compared to the rDNA oligonucleotide, similar to the results for 1:5 protein:DNA molar ratio (Figure 10A and Supplementary Figure S10A). nPfh1 hydrolyzed ~0.3 nmoles ATP, which significantly decreased in the presence of Phen-DC_3 ($P < 0.04$), suggesting that a stabilized G4 structure reduces the amount of ATP hydrolyzed by nPfh1 (Figure 10B). We also tested ATP hydrolysis on the less stable rDNA-m4 substrate, which led to 5-fold higher levels of ATP hydrolysis again showing that the ATPase activity of nPfh1 was inhibited by the stable rDNA G4 structure. In addition, the presence of Phen-DC_3 significantly reduced the amount of ATP hydrolyzed by nPfh1 on the rDNA-m4 substrate ($P < 0.04$), demonstrating that Phen-DC_3–induced G4 structures also inhibit the ATP hydrolysis by nPfh1 (Figure 10B). The detected ATP hydrolysis was due to the ATPase activity of nPfh1 and not to protein impurities, because nPfh1-K338A had no or negligible ATPase activity compared to nPfh1 for all three tested oligonucleotides (Supplementary Figure S10A).

The ATP hydrolysis for the telomeric oligonucleotide was lower than for the rDNA oligonucleotide. However, the amount of hydrolyzed ATP increased dramatically to similar levels for the telomere-m4 oligonucleotide as for the rDNA-m4 oligonucleotide (Figure 10B). Although ATP hydrolysis by nPfh1 on the telomeric oligonucleotide was unaffected by Phen-DC_3 treatment, a 3-fold inhibition of ATP hydrolysis was detected with the Phen-DC_3-treated telomere-m4 oligonucleotide, which can be explained by the slight G4-inducing ability of Phen-DC_3, as shown by the CD analysis (Figure 8B). Finally, the ATP hydrolysis of nPfh1 was tested in the absence of salt to determine if the low levels of ATP hydrolysis were due to the formation of G4 structures. Indeed, ATP hydrolysis by nPfh1 was at a similar level for the rDNA and telomeric oligonucleotides compared to three different (24, 57 and 75 nt; see Supplementary Table S1) non-G4 oligonucleotides (Supplementary Figure S10B), confirming that G4 structures indeed inhibit ATP hydrolysis by nPfh1.

DISCUSSION

The past decade has witnessed an increasing amount of support for the existence of G4 motifs in different organisms and thus the importance of G4 structures. Recently, two studies suggested the presence of G4 structures in the *S. pombe* genome (7,53). In the first study, a bioinformatics analysis combined with ChIP-seq demonstrated that Pfh1 is enriched at G4 motifs to prevent fork pausing and DNA damage at these sites, and it also showed that G4 motifs are evolutionarily conserved at telomeric DNA, rDNA and promoter regions (7). In the second study, the Rif1 protein, a telomere- and origin-associated protein, was shown to bind G4 structures formed by a non-typical G4 motif, which was required to prevent origin firing (53). In addition, a recent study showed that short telomere length phenotype in *rpa-D223Y S. pombe* cells can be rescued when overexpressing Pif1 helicases from different organisms, including Pfh1 and hPIF1, under the strong *nmt1* promoter. This sug-

gests that the binding of RPA (ssDNA-binding protein) to telomeres prevents formation of secondary structures, perhaps including G4 structures (54).

Here, we conducted several biophysical and biochemical assays as well as *in vivo* experiments to investigate the formation of G4 structures at two G4 motif-enriched regions in the genetically tractable model organism *S. pombe*. We provide several pieces of strong evidence that these DNA sequences in the rDNA and telomeric regions adopt G4 structures. The stability and conformation of the G4 structures were dependent on both the sequence of the G4 motifs and whether Na^+ or K^+ was used during the folding of the oligonucleotides. By using CD analysis, we found that a G4 motif from rDNA adopts a stable parallel G4 structure in the presence of both cation species.

The telomeric oligonucleotide used in this study could only form a stable G4 structure when folded in the presence of K^+. The peak from the CD spectra of this oligonucleotide was broader than that of a typical parallel G4 structure suggesting that the oligonucleotide adopted either a mixture of parallel and antiparallel structures or a hybrid conformation. Previously, an oligonucleotide from the *S. pombe* telomeric region with the sequence $(GGTTAC)_3GG$ was shown to only adopt a G4 structure at 4°C and to have very low thermal stability with an estimated T_m of ∼27°C (55). In this study, we selected a telomeric oligonucleotide from an 18 kb sequenced telomeric DNA library (7,56) and found that the formed G4 structure was stable at physiologically relevant temperatures and was much more resistant to thermal unfolding (T_m ∼51°C).

By using two different methods — CD analysis of the T_m of the oligonucleotides and native gels — we demonstrated that the rDNA oligonucleotide forms intermolecular G4 structures and that the telomeric oligonucleotide adopts an intramolecular G4 structure. These results could potentially reflect the organization of the sequences in the genome; the rDNA region might have a higher propensity to fold into intermolecular G4 structures due to the high copy number of the rDNA loci, whereas although the telomeric DNA is a repetitive sequence, the number of repeats is much lower compared to the rDNA repeats and therefore it is more inclined toward the formation of an intramolecular G4 structure. In fact, although different studies have shown that human telomeric DNA can adopt several different G4 topologies, many of them demonstrated that the sequences form intramolecular G4 structures (57–60).

Unresolved G4 structures are obstacles to replication and transcription machineries *in vivo*. We confirmed by ChIP-qPCR that the *S. pombe* Pif1 family member Pfh1 is enriched at the telomeres (42), and the rDNA G4 motif. The association occurs during S phase—when the G4 motifs have a higher propensity to form G4 structures due to higher abundance of ssDNA—because Pfh1-Myc was enriched at these sites during mid to late S phase.

To investigate whether Pfh1 could bind and unwind stably formed G4 structures, we focused on the nuclear isoform of the protein because this isoform has not been previously purified and studied. Also, the G4 structures were formed from G4 motifs derived from the rDNA and telomeric regions which are located in the nucleus. Previous studies either failed to purify satisfying amounts of active Pfh1 or had to resort to truncation of the protein due to solubility and degradation problems (32,33). However, Seo *et al.* finally purified Pfh1 corresponding to the full-length ORF with NusA as a carrier protein (31). To optimize the expression and solubility of nPfh1, we co-expressed nPfh1 with various carrier proteins in *E. coli* using different concentrations of IPTG as well as by varying the induction time and inducing expression at 20°C or 37°C. In the end, we were able to purify active nPfh1 using Trx (∼14 kDa), a much smaller protein than NusA (∼60 kDa), with a yield of ∼0.15 mg protein per liter of *E. coli* cells.

The recombinant nPfh1 displayed a strong binding affinity to the intermolecular rDNA G4 folded in either NaCl or KCl. However, the protein bound weakly to the intramolecular telomeric G4. Compared to both a partial duplex DNA substrate with the same $poly(A)_{10}$ overhang as the G4 DNA substrates and a $poly(A)_{10}$ oligo, nPfh1 had a slightly higher binding affinity for the intramolecular telomeric G4 structure, suggesting that the G4-binding preference of nPfh1 is similar to ScPif1 (47). Pfh1 had a higher occupancy at the telomeres compared to the rDNA G4 motif *in vivo* and this may be due to Pfh1's other functions in the cell, such as potentially removing non-nucleosomal protein obstacles and not only due to its G4 unwinding activity.

nPfh1 efficiently unwound the rDNA G4 oligonucleotide folded in NaCl, even in the presence of trap DNA, indicating processive helicase activity that is more similar to ScPif1 than to bacterial Pif1 helicases (20). In contrast, the rDNA G4 oligonucleotide folded in KCl proved to be more resistant to unwinding by the protein. These results are consistent with the CD data analysis where KCl conferred a higher stabilization effect compared to NaCl, which has been attributed to the greater energetic cost of dehydrating Na^+ compared to K^+ (61). ScPif1 has a stronger preference for G4 DNA folded in NaCl compared to other forms of DNA secondary structures (20), whereas the bacterial BsPif1 (30) and hPIF1 (17) unwind partial duplex DNA as efficiently or less efficiently than G4 substrates folded in KCl or a mixture of NaCl and KCl. Therefore, to investigate the DNA substrate preference of nPfh1, the unwinding of the partial duplex DNA substrate with the same $poly(A)_{10}$ overhang as the G4 oligonucleotides was assessed. nPfh1 displayed a similar helicase activity as for the telomeric G4 oligonucleotide, i.e. considerably lower unwinding efficiency than for the rDNA G4 in NaCl, but substantially higher helicase activity compared to the rDNA in KCl. These observations demonstrate that the unwinding efficiency of G4 structures by nPfh1 strongly depends on the structure and the intrinsic stability of the G4 structure. Also, it suggests that there is a difference in the efficiency of unwinding G4 structures by different Pif1 family members. The diverse N- and C-termini of different Pif1 helicases might play important roles in the differences found in G4 unwinding. However, these variations in unwinding capacity can perhaps also be due to the different G4 structures used in the different studies as well as to which cations were used to fold the G4 structures.

The well-studied G4-binding molecule Phen-DC_3 is a highly effective G4 DNA stabilizer, and we found that the addition of the compound increased the thermal stability of both the rDNA and telomeric G4 structures. For the telom-

eric G4 structure, Phen-DC_3 also induced a partial structural change from a predominantly parallel structure to a hybrid or mixed population of parallel and antiparallel conformations. This conformational change was also observed for human intramolecular G4 structures and has been ascribed to the outcompeting effect of the G4 ligand on the K^+ ions (51,62). Importantly, as indicated from the CD and ATPase experiments using the rDNA-m4 sequence, Phen-DC_3 could also partially induce G4 formation for a G-rich non-G4 motif oligonucleotide. Hence, to reduce false-positive results the potential of inducing G4 structures in G-rich sequences when using G4-binding compounds should always be considered.

nPfh1 was still able to unwind the G4 structures despite being stabilized by Phen-DC_3, demonstrating the G4 resolving efficiency of the protein. Importantly, Phen-DC_3 only affected the G4 DNA and did not have any impact on the helicase activity of nPfh1. Surprisingly, the presence of Phen-DC_3 did not lead to a lower unwinding efficiency for the rDNA sequence folded in KCl even though the thermal stability of the G4 structure — as inferred from the CD analysis — had increased. Therefore, the stabilization effect of Phen-DC_3 might differ depending on whether the G4 structure is thermally melted or unwound by a helicase. The unwinding inhibition of nPfh1 by Phen-DC_3 appears to be influenced by the specific structure formed by the G4 motif as well as to its robustness *per se*, because Phen-DC_3 had a stronger inhibitory effect on nPfh1 for the intramolecular telomeric G4 structures compared to the intermolecular rDNA G4 oligonucleotide folded in NaCl but had no effect on the much more stable rDNA G4 in KCl. The lack of effect of Phen-DC_3 on the stability of the rDNA G4 folded in KCl in the unwinding experiments can potentially be due to the intrinsically high stability of the G4 structure, because even in the absence of Phen-DC_3 it was very resistant to boiling (middle panel in Supplementary Figure S7). Furthermore, the more G4-stabilizing buffer conditions (presence of Mg^{2+}, higher KCl to DNA molar ratio) compared to the CD measurements, could explain the discrepancy between the results from the unwinding (±Phen-DC_3) and CD experiments (±Phen-DC_3).

Helicases are dependent on the hydrolysis of ATP molecules to drive the unwinding of duplex DNA, and the amount of hydrolyzed ATP is correlated to how easily the helicase can translocate on the ssDNA as well as the potential requirement of an energy source for active strand separation. The presence of stable DNA secondary structures would therefore be expected to lower the ATP consumption. Evidently, nPfh1 hydrolyzed smaller amounts of ATP molecules in the presence of G4 substrates compared to ssDNA of various lengths. This ATPase inhibition imposed by G4 structures may not solely be explained by the fact that they create physical obstacles that prevent proteins from translocating along the DNA and therefore fall off. Indeed, ScPif1 had a lower rate of ATP hydrolysis in the presence of an intramolecular G4 structure compared to a single-stranded oligonucleotide of the same length as the single-stranded overhang of the G4 structure, despite the fact that ScPif1 exhibited a much lower K_d for the G4 substrate. (47). Similar to ScPif1, nPfh1 displayed a greater binding affinity to the intramolecular telomeric G4 structure compared to the ssDNA substrate of the same length as the G4 structure overhang. A possible scenario could be that when there is a G4 structure present and the protein concentration is too low for efficient unwinding, the helicase is bound at the ssDNA–G4 junction and therefore performs little translocation activity, while the helicase more repeatedly binds, translocates on, and falls off the ssDNA substrate.

The ATP hydrolysis for the telomeric G4 substrate was lower than for the rDNA G4 substrate, which was probably due to the fact that the rDNA sequence formed intermolecular G4 structures, while the telomeric sequence folded into an intramolecular G4 structure. Indeed, unwinding an intermolecular G4 structure would lead to the formation of several ssDNA strands available for free translocation by nPfh1, while unwinding an intramolecular G4 structure would only yield one ssDNA, providing less template for the helicase to translocate on. This would also explain the observed higher binding affinity of nPfh1 to the rDNA G4 structure compared to the G4 structure adopted by the telomeric oligonucleotide. The ATPase activity of nPfh1 on the G4 substrate reached a similar level as the non-G4 oligonucleotide when the protein:DNA ratio was shifted toward more protein. At these protein levels, nPfh1 might translocate on the substrates to keep the DNA single-stranded. In fact, single-molecule analysis has shown that ScPif1 patrols DNA containing G4 motifs by reeling in the DNA to prevent G4 structures from forming (41).

In conclusion, G4 motifs can adopt a wide array of structures that are associated with many biological functions, including telomere maintenance, gene regulation, and origin firing. Our work demonstrates that G4 motifs in the *S. pombe* rDNA and telomeric regions have high Pfh1 occupancy *in vivo* and that they fold into stable G4 structures *in vitro*. The nuclear isoform of Pfh1 can bind and resolve these structures, even when they are stabilized by Phen-DC_3. Because G4 motifs in telomeres and rDNA are conserved, our results suggest that these structures play important functions *in vivo*. Our study adds another helicase to the list of efficient G4 unwinders and provides further evidence for the evolutionarily conserved role of Pif1 helicases as potent unwinders of G4 structures.

SUPPLEMENTARY DATA

Supplementary Data are available at NAR Online.

ACKNOWLEDGEMENTS

We thank Dr Marie-Paule Teulade-Fichou (Institut Curie, France) for kindly sending us Phen-DC_3 and Gunter Stier (Universität Heidelberg, Germany) for providing us the modified pET-22b vectors. We are also grateful to Dr Phong Lan Thao Tran (Princeton University, USA) for her excellent advices regarding the setup of the G4 molecularity experiment and Dr Ikenna Obi (Umeå University, Sweden) for his assistance in setting up the ATPase assay.

FUNDING

Swedish Research Council; The Kempe Foundations [JCK-1325]; Swedish Society for Medical Research; Wenner-

Gren Foundations; The Kempe Foundations [SMK-1246 to M.W.]; Wenner-Gren Foundations (to K.P.Y.). Funding for open access charge: Swedish Research Council.
Conflict of interest statement. None declared.

REFERENCES

1. Bochman,M.L., Paeschke,K. and Zakian,V.A. (2012) DNA secondary structures: stability and function of G-quadruplex structures. *Nat. Rev. Genet.*, **13**, 770–780.
2. Capra,J.A., Paeschke,K., Singh,M. and Zakian,V.A. (2010) G-quadruplex DNA sequences are evolutionarily conserved and associated with distinct genomic features in *Saccharomyces cerevisiae*. *PLoS Comput. Biol.*, **6**, e1000861.
3. Hershman,S.G., Chen,Q., Lee,J.Y., Kozak,M.L., Yue,P., Wang,L.S. and Johnson,F.B. (2008) Genomic distribution and functional analyses of potential G-quadruplex-forming sequences in *Saccharomyces* cerevisiae. *Nucleic Acids Res.*, **36**, 144–156.
4. Rawal,P., Kummarasetti,V.B., Ravindran,J., Kumar,N., Halder,K., Sharma,R., Mukerji,M., Das,S.K. and Chowdhury,S. (2006) Genome-wide prediction of G4 DNA as regulatory motifs: role in *Escherichiacoli* global regulation. *Genome Res.*, **16**, 644–655.
5. Todd,A.K., Johnston,M. and Neidle,S. (2005) Highly prevalent putative quadruplex sequence motifs in human DNA. *Nucleic Acids Res.*, **33**, 2901–2907.
6. Huppert,J.L. and Balasubramanian,S. (2005) Prevalence of quadruplexes in the human genome. *Nucleic Acids Res.*, **33**, 2908–2916.
7. Sabouri,N., Capra,J.A. and Zakian,V.A. (2014) The essential *Schizosaccharomyces pombe* Pfh1 DNA helicase promotes fork movement past G-quadruplex motifs to prevent DNA damage. *BMC Biol.*, **12**, 101.
8. Huppert,J.L. and Balasubramanian,S. (2007) G-quadruplexes in promoters throughout the human genome. *Nucleic Acids Res.*, **35**, 406–413.
9. Drygin,D., Siddiqui-Jain,A., O'Brien,S., Schwaebe,M., Lin,A., Bliesath,J., Ho,C.B., Proffitt,C., Trent,K., Whitten,J.P. *et al.* (2009) Anticancer activity of CX-3543: a direct inhibitor of rRNA biogenesis. *Cancer Res.*, **69**, 7653–7661.
10. Chambers,V.S., Marsico,G., Boutell,J.M., Di Antonio,M., Smith,G.P. and Balasubramanian,S. (2015) High-throughput sequencing of DNA G-quadruplex structures in the human genome. *Nat. Biotechnol.*, **33**, 877–881.
11. Biffi,G., Tannahill,D., McCafferty,J. and Balasubramanian,S. (2013) Quantitative visualization of DNA G-quadruplex structures in human cells. *Nat. Chem.*, **5**, 182–186.
12. Henderson,A., Wu,Y., Huang,Y.C., Chavez,E.A., Platt,J., Johnson,F.B., Brosh,R.M. Jr, Sen,D. and Lansdorp,P.M. (2013) Detection of G-quadruplex DNA in mammalian cells. *Nucleic Acids Res.*, **42**, 860–869.
13. Hoffman,C.S., Wood,V. and Fantes,P.A. (2015) An ancient yeast for young geneticists: a primer on the *Schizosaccharomyces pombe* model system. *Genetics*, **201**, 403–423.
14. Smith,J.S., Chen,Q., Yatsunyk,L.A., Nicoludis,J.M., Garcia,M.S., Kranaster,R., Balasubramanian,S., Monchaud,D., Teulade-Fichou,M.P., Abramowitz,L. *et al.* (2011) Rudimentary G-quadruplex-based telomere capping in *Saccharomyces cerevisiae*. *Nat. Struct. Mol. Biol.*, **18**, 478–485.
15. Zahler,A.M., Williamson,J.R., Cech,T.R. and Prescott,D.M. (1991) Inhibition of telomerase by G-quartet DNA structures. *Nature*, **350**, 718–720.
16. Maizels,N. (2015) G4-associated human diseases. *EMBO Rep.*, **16**, 910–922.
17. Sanders,C.M. (2010) Human Pif1 helicase is a G-quadruplex DNA-binding protein with G-quadruplex DNA-unwinding activity. *Biochem. J.*, **430**, 119–128.
18. Chisholm,K.M., Aubert,S.D., Freese,K.P., Zakian,V.A., King,M.C. and Welcsh,P.L. (2012) A genomewide screen for suppressors of *Alu*-mediated rearrangements reveals a role for PIF1. *PLoS One*, **7**, e30748.
19. Bochman,M.L., Sabouri,N. and Zakian,V.A. (2010) Unwinding the functions of the Pif1 family helicases. *DNA Repair*, **9**, 237–249.
20. Paeschke,K., Bochman,M.L., Garcia,P.D., Cejka,P., Friedman,K.L., Kowalczykowski,S.C. and Zakian,V.A. (2013) Pif1 family helicases suppress genome instability at G-quadruplex motifs. *Nature*, **497**, 458–462.
21. Sabouri,N., McDonald,K.R., Webb,C.J., Cristea,I.M. and Zakian,V.A. (2012) DNA replication through hard-to-replicate sites, including both highly transcribed RNA Pol II and Pol III genes, requires the *S. pombe* Pfh1 helicase. *Genes Dev.*, **26**, 581–593.
22. Ivessa,A.S., Zhou,J.Q., Schulz,V.P., Monson,E.K. and Zakian,V.A. (2002) *Saccharomyces* Rrm3p, a 5′ to 3′ DNA helicase that promotes replication fork progression through telomeric and subtelomeric DNA. *Genes Dev.*, **16**, 1383–1396.
23. Ivessa,A.S., Lenzmeier,B.A., Bessler,J.B., Goudsouzian,L.K., Schnakenberg,S.L. and Zakian,V.A. (2003) The *Saccharomyces cerevisiae* helicase Rrm3p facilitates replication past nonhistone protein-DNA complexes. *Mol. Cell*, **12**, 1525–1536.
24. Ivessa,A.S., Zhou,J.Q. and Zakian,V.A. (2000) The *Saccharomyces* Pif1p DNA helicase and the highly related Rrm3p have opposite effects on replication fork progression in ribosomal DNA. *Cell*, **100**, 479–489.
25. Paeschke,K., Capra,J.A. and Zakian,V.A. (2011) DNA replication through G-quadruplex motifs is promoted by the *Saccharomyces cerevisiae* Pif1 DNA helicase. *Cell*, **145**, 678–691.
26. Ribeyre,C., Lopes,J., Boule,J.B., Piazza,A., Guedin,A., Zakian,V.A., Mergny,J.L. and Nicolas,A. (2009) The yeast Pif1 helicase prevents genomic instability caused by G-quadruplex-forming CEB1 sequences *in vivo*. *PLoS Genet.*, **5**, e1000475.
27. Lopes,J., Piazza,A., Bermejo,R., Kriegsman,B., Colosio,A., Teulade-Fichou,M.P., Foiani,M. and Nicolas,A. (2011) G-quadruplex-induced instability during leading-strand replication. *EMBO J.*, **30**, 4033–4046.
28. Piazza,A., Serero,A., Boule,J.B., Legoix-Ne,P., Lopes,J. and Nicolas,A. (2012) Stimulation of gross chromosomal rearrangements by the human CEB1 and CEB25 minisatellites in *Saccharomyces cerevisiae* depends on G-quadruplexes or Cdc13. *PLoS Genet.*, **8**, e1003033.
29. Pinter,S.F., Aubert,S.D. and Zakian,V.A. (2008) The *Schizosaccharomyces pombe* Pfh1p DNA helicase is essential for the maintenance of nuclear and mitochondrial DNA. *Mol. Cell. Biol.*, **28**, 6594–6608.
30. Liu,N.N., Duan,X.L., Ai,X., Yang,Y.T., Li,M., Dou,S.X., Rety,S., Deprez,E. and Xi,X.G. (2015) The *Bacteroides sp. 3_1_23* Pif1 protein is a multifunctional helicase. *Nucleic Acids Res.*, **43**, 8942–8954.
31. Ryu,G.H., Tanaka,H., Kim,D.H., Kim,J.H., Bae,S.H., Kwon,Y.N., Rhee,J.S., MacNeill,S.A. and Seo,Y.S. (2004) Genetic and biochemical analyses of Pfh1 DNA helicase function in fission yeast. *Nucleic Acids Res.*, **32**, 4205–4216.
32. Zhou,J.Q., Qi,H., Schulz,V.P., Mateyak,M.K., Monson,E.K. and Zakian,V.A. (2002) *Schizosaccharomyces pombe pfh1*$^+$ encodes an essential 5′ to 3′ DNA helicase that is a member of the PIF1 subfamily of DNA helicases. *Mol. Biol. Cell*, **13**, 2180–2191.
33. Tanaka,H., Ryu,G.H., Seo,Y.S., Tanaka,K., Okayama,H., MacNeill,S.A. and Yuasa,Y. (2002) The fission yeast *pfh1*$^+$ gene encodes an essential 5′ to 3′ DNA helicase required for the completion of S-phase. *Nucleic Acids Res.*, **30**, 4728–4739.
34. Renaud de la Faverie,A., Guedin,A., Bedrat,A., Yatsunyk,L.A. and Mergny,J.L. (2014) Thioflavin T as a fluorescence light-up probe for G4 formation. *Nucleic Acids Res.*, **42**, e65.
35. Paramasivan,S., Rujan,I. and Bolton,P.H. (2007) Circular dichroism of quadruplex DNAs: applications to structure, cation effects and ligand binding. *Methods*, **43**, 324–331.
36. Williamson,J.R. (1994) G-quartet structures in telomeric DNA. *Annu. Rev. Biophys. Biomol. Struct.*, **23**, 703–730.
37. Mohanty,J., Barooah,N., Dhamodharan,V., Harikrishna,S., Pradeepkumar,P.I. and Bhasikuttan,A.C. (2013) Thioflavin T as an efficient inducer and selective fluorescent sensor for the human telomeric G-quadruplex DNA. *J. Am. Chem. Soc.*, **135**, 367–376.
38. Oganesian,L., Moon,I.K., Bryan,T.M. and Jarstfer,M.B. (2006) Extension of G-quadruplex DNA by ciliate telomerase. *EMBO J.*, **25**, 1148–1159.
39. Rhodes,D. and Lipps,H.J. (2015) G-quadruplexes and their regulatory roles in biology. *Nucleic Acids Res.*, **43**, 8627–8637.
40. Duan,X.L., Liu,N.N., Yang,Y.T., Li,H.H., Li,M., Dou,S.X. and Xi,X.G. (2015) G-quadruplexes significantly stimulate Pif1

helicase-catalyzed duplex DNA unwinding. *J. Biol. Chem.*, **290**, 7722–7735.
41. Zhou,R., Zhang,J., Bochman,M.L., Zakian,V.A. and Ha,T. (2014) Periodic DNA patrolling underlies diverse functions of Pif1 on R-loops and G-rich DNA. *Elife*, **3**, e02190.
42. McDonald,K.R., Sabouri,N., Webb,C.J. and Zakian,V.A. (2014) The Pif1 family helicase Pfh1 facilitates telomere replication and has an RPA-dependent role during telomere lengthening. *DNA Repair*, **24**, 80–86.
43. Webb,C.J. and Zakian,V.A. (2012) *Schizosaccharomyces pombe* Ccq1 and TER1 bind the 14-3-3-like domain of Est1, which promotes and stabilizes telomerase-telomere association. *Genes Dev.*, **26**, 82–91.
44. Tomita,K. and Cooper,J.P. (2008) Fission yeast Ccq1 is telomerase recruiter and local checkpoint controller. *Genes Dev.*, **22**, 3461–3474.
45. Calero,F., Gomez,N., Arino,J. and Ramos,J. (2000) Trk1 and Trk2 define the major K^+ transport system in fission yeast. *J. Bacteriol.*, **182**, 394–399.
46. Rothe,M. and Hofer,M. (1994) K^+-Fluxes and Growth of *Schizosaccharomyces Pombe* at Various External K^+-Concentrations. *Folia Microbiol.*, **39**, 543–545.
47. Byrd,A.K. and Raney,K.D. (2015) A parallel quadruplex DNA is bound tightly but unfolded slowly by pif1 helicase. *J. Biol. Chem.*, **290**, 6482–6494.
48. Salvati,E., Zizza,P., Rizzo,A., Iachettini,S., Cingolani,C., D'Angelo,C., Porru,M., Randazzo,A., Pagano,B., Novellino,E. *et al.* (2014) Evidence for G-quadruplex in the promoter of *vegfr-2* and its targeting to inhibit tumor angiogenesis. *Nucleic Acids Res.*, **42**, 2945–2957.
49. Balasubramanian,S., Hurley,L.H. and Neidle,S. (2011) Targeting G-quadruplexes in gene promoters: a novel anticancer strategy? *Nat. Rev. Drug Discov.*, **10**, 261–275.
50. Piazza,A., Boule,J.B., Lopes,J., Mingo,K., Largy,E., Teulade-Fichou,M.P. and Nicolas,A. (2010) Genetic instability triggered by G-quadruplex interacting Phen-DC compounds in *Saccharomyces cerevisiae*. *Nucleic Acids Res.*, **38**, 4337–4348.
51. Boncina,M., Podlipnik,C., Piantanida,I., Eilmes,J., Teulade-Fichou,M.P., Vesnaver,G. and Lah,J. (2015) Thermodynamic fingerprints of ligand binding to human telomeric G-quadruplexes. *Nucleic Acids Res.*, **43**, 10376–10386.
52. Chung,W.J., Heddi,B., Hamon,F., Teulade-Fichou,M.P. and Phan,A.T. (2014) Solution structure of a G-quadruplex bound to the bisquinolinium compound Phen-DC_3. *Angew. Chem.*, **53**, 999–1002.
53. Kanoh,Y., Matsumoto,S., Fukatsu,R., Kakusho,N., Kono,N., Renard-Guillet,C., Masuda,K., Iida,K., Nagasawa,K., Shirahige,K. *et al.* (2015) Rif1 binds to G quadruplexes and suppresses replication over long distances. *Nat. Struct. Mol. Biol.*, **22**, 889–897.
54. Audry,J., Maestroni,L., Delagoutte,E., Gauthier,T., Nakamura,T.M., Gachet,Y., Saintome,C., Geli,V. and Coulon,S. (2015) RPA prevents G-rich structure formation at lagging-strand telomeres to allow maintenance of chromosome ends. *EMBO J.*, **34**, 1942–1958.
55. Tran,P.L., Mergny,J.L. and Alberti,P. (2011) Stability of telomeric G-quadruplexes. *Nucleic Acids Res.*, **39**, 3282–3294.
56. Webb,C.J. and Zakian,V.A. (2015) Telomerase RNA stem terminus element affects template boundary element function, telomere sequence, and shelterin binding. *Proc. Natl. Acad. Sci. U.S.A.*, **112**, 11312–11317.
57. Ambrus,A., Chen,D., Dai,J., Bialis,T., Jones,R.A. and Yang,D. (2006) Human telomeric sequence forms a hybrid-type intramolecular G-quadruplex structure with mixed parallel/antiparallel strands in potassium solution. *Nucleic Acids Res.*, **34**, 2723–2735.
58. He,Y., Neumann,R.D. and Panyutin,I.G. (2004) Intramolecular quadruplex conformation of human telomeric DNA assessed with ^{125}I-radioprobing. *Nucleic Acids Res.*, **32**, 5359–5367.
59. Phan,A.T., Luu,K.N. and Patel,D.J. (2006) Different loop arrangements of intramolecular human telomeric (3+1) G-quadruplexes in K^+ solution. *Nucleic Acids Res.*, **34**, 5715–5719.
60. Lane,A.N. (2012) The stability of intramolecular DNA G-quadruplexes compared with other macromolecules. *Biochimie*, **94**, 277–286.
61. Hud,N.V., Smith,F.W., Anet,F.A. and Feigon,J. (1996) The selectivity for K^+ versus Na^+ in DNA quadruplexes is dominated by relative free energies of hydration: a thermodynamic analysis by ^{1}H NMR. *Biochemistry*, **35**, 15383–15390.
62. Marchand,A., Granzhan,A., Iida,K., Tsushima,Y., Ma,Y., Nagasawa,K., Teulade-Fichou,M.P. and Gabelica,V. (2015) Ligand-induced conformational changes with cation ejection upon binding to human telomeric DNA G-quadruplexes. *J. Am. Chem. Soc.*, **137**, 750–756.